Al and Sr environment in tectosilicate glasses and melts: Viscosity, Raman and NMR investigation

Alexey Novikov, Daniel R. Neuville, Louis Hennet, Yann Gueguen, Dominique Thiaudière, Thibault Charpentier, Pierre Florian

Al and Sr environment in tectosilicate glasses and melts: viscosity, Raman and NMR investigation

Alexey N. Novikov[1,2*], Daniel R. Neuville[2*], Louis Hennet[1], Yann Gueguen[3], Dominique Thiaudière[4], Thibault Charpentier[5], Pierre Florian[1]

1 – CEMHTI UPR3079 CNRS, Univ. Orléans, F-45071 Orléans, France

2 – IPGP UMR7154 CNRS, Géomatériaux, Paris Sorbonne Cité, 75005 Paris, France

3 – IPR UMR UR1-CNRS 6251, Université de Rennes 1, 35042 Rennes, France

4 – Synchrotron SOLEIL, 91192 Gif-sur-Yvette, France

5 – NIMBE, CEA, CNRS, Université Paris-Saclay, CEA Saclay, 91191 Gif-sur-Yvette cedex, France

*alexey.novikov@cnrs-orleans.fr and neuville@ipgp.fr

Abstract

Structure and properties of SrO-Al_2O_3-SiO_2 glasses and melts were investigated along the tectosilicate join ($SrO/Al_2O_3 = 1$), varying the amount of silica. The structure of the glasses was studied by means of various spectroscopic techniques: Raman, ^{27}Al NMR and XAS at the Sr K-edge. Raman spectroscopy revealed that the fraction of high-membered tetrahedral rings diminishes upon substitution of SiO_2 by $SrAl_2O_4$ favouring the formation of low-membered rings. Sr K-edge XANES shows that the strontium coordination number is around 9, based on the spectrum similarity with the one obtained for crystalline strontianite. ^{27}Al NMR spectroscopy indicates the presence of four- and five-coordinated aluminium the latter being found in small quantities (< 5 %), i.e. smaller than for analogous Mg- and Ca-based aluminosilicate glasses. A minimum in T_g is found when the AlO_5 content is maximum, both in Sr and Ca aluminosilicates. This fact indicates the importance of minor species such as five-fold aluminium in activating viscous flow, similarly to what has been proposed for five-fold silicon by Farnan and Stebbins (1994). Increase of T_g at low silica content was correlated to a decrease in AlO_5 content as well as to a decrease of a number of different structural units and, as a consequence, an ordering of the system.

Keywords: strontium glasses; aluminosilicates; viscosity; configurational entropy; five-fold aluminium; structure

Highlights

- Macroscopic and nanoscopic investigations of strontium tectosilicates.
- Viscosity, density and glass transition temperature measurements.
- Structure at short and medium range order by Raman, ^{27}Al NMR and XAS.

1. INTRODUCTION

Strontium is an element whose abundance in Earth's crust is at the level of 300-400 ppm (Turekian and Kulp, 1956; Turekian and Wedepohl, 1961; Taylor, 1964; Rudnick and Gao, 2003). In earth science, strontium can be used as a Sr/Rb geochronometer, for studying the petrogenesis of igneous rocks and for tracing weathering processes (Moorbath et al., 1977; Capo et al., 1998). It is also possible to date rocks formation by measuring the ratio of non-radiogenic ^{86}Sr to radiogenic ^{87}Sr (resulting from the radioactive decay of ^{87}Rb). But Sr and Rb follow different behaviour during fractional crystallization: the former goes preferentially in early-formed calcic plagioclase while the latter concentrates in the residual magma and enters later potassium minerals (Faure and Powell, 1972; DePaolo, 1981). In material sciences, Sr aluminosilicate glasses, glass-ceramics and ceramics have shown applications as transparent ceramics (Al Saghir et al., 2015), high-temperature sealants (Sharma et al., 2012) and refractory materials (Hyatt and Bansal, 1996; Bansal, 1998; Beall, 2009).

To better understand natural and industrial processes, it is important to link macroscopic properties (density, viscosity, glass transition temperature etc.) of the glasses/ceramics with the structure of the corresponding melts. Some investigations in this field have been already made for Na-based (Furukawa et al., 1981; Seifert et al., 1982; Fukumi et al., 1990; Mysen, 1990; Merzbacher and White, 1991; Mysen and Frantz, 1993; Mysen and Frantz, 1994; Mysen, 1999; Allwardt et al., 2005a,b; Le Losq et al., 2014), Mg-based (Seifert et al., 1982; Merzbacher and White, 1991; Neuville et al., 2008a) and Ca-based aluminosilicates (Seifert et al., 1982; Frantz and Mysen, 1995; Allwardt et al., 2005b; Kanehashi and Stebbins, 2007; Neuville et al., 2004a,b, 2006, 2008b, 2010; Drewitt et al., 2012; Jakse et al., 2014; Hennet et al., 2016) using a multi-technique approach. The SrO-Al_2O_3-SiO_2 (SAS) ternary system is, on the other hand, poorly studied. There are only a handful of studies in this system and most of them concentrate only on specific properties and have used only few techniques (see for example Bockris et al., 1955; Chiari et al., 1975; Magaritz and Hofmann, 1978; Creux et al., 1995; Neuville, 2005; Licheron et al., 2011; Abel et al., 2013).

In order to connect structural features with macroscopic properties of Sr aluminosilicates we intend to apply a multi-technique approach for studying tectosilicate compositions. This approach consists of measuring density and viscosity as well as spectroscopic techniques such as Raman, NMR and X-ray absorption spectroscopy. We also intend to compare the effect of Sr on the aluminosilicate network with the well-studied ones of Mg and Ca, recalling that strontium is a heavier element possessing a bigger radius than the two latter cations. Those differences are expected to affect the properties and structure of the melts and corresponding glasses/ceramics like potassium does, i.e. by greatly disturbing the network and increasing its topological and chemical disorder (Le Losq and Neuville, 2013; Le Losq et al., 2016).

2. EXPERIMENTAL METHODS

2.1 Starting materials

Strontium aluminosilicate samples were made by a traditional melting-quenching procedure described in Neuville (2006). For this, powders of Rectapur reagents from Merck were pre-dried at 1000 °C (SiO_2, Al_2O_3) and 550 °C ($SrCO_3$) before being mixed at a stoichiometric amount and crushed together in an agate mortar under ethanol for 1 h. Then the mixture was slowly heated in a platinum crucible up to 1100-1250 °C in an electric muffle furnace and held at that temperature for several hours to decompose the carbonate. After the decarbonation step, mixtures were melted at 1600 °C and quenched either by dipping the bottom of the crucible in water if the viscosity of the melt was high or by pouring the melt on a large copper plate if the viscosity was low. The grinding, melting, quenching procedures were repeated three times to ensure the homogeneity of the final product. Compositions were maintained at a temperature above their melting points for several hours to produce bubble-free samples for further viscosity measurements. In the cases when glass samples could not be obtained by traditional quenching (i.e. SA10.45, SA20.40, SA50.25 and SA57.21 samples), ceramic compositions were prepared following the above described procedure and an aerodynamic levitation device coupled with two CO_2 lasers was used to prepare small glass spheres (Hennet et al., 2006; Neuville et al., 2006, 2008a, 2014). To be sure that those two quenching procedures did not affect the properties and structure of the glasses, two samples of a SAS glass obtained by traditional and "levitation" quench were studied. ^{27}Al NMR and Raman spectroscopies as well as density measurements did not reveal any differences in the samples. So, we assume further that for the studied samples the quenching method did not cause significant differences in the structure and properties.

All samples were checked to be free of a crystalline phase. For this, several pieces of each composition were studied microscopically and by means of Raman spectroscopy. Densities measured with the Archimedean method using toluene as the immersion liquid of those pieces were also measured and are found to be approximately identical for each composition. Chemical compositions (Table 1) were measured using a Cameca SX100 electron probe microanalyser with a 10 nA current, accelerating voltage of 15 kV and 90 s counting time. Each composition is an average of 5-10 measurements. The names of the glasses are given by SAxx.yy, where xx is the SiO_2 content in mol%, yy is the Al_2O_3 content in mol%, the remaining being the content of SrO.

2.2 Viscosity measurements

Creep apparatus: the viscosity measurements at low temperatures were performed using a creep apparatus (Neuville and Richet, 1991; Neuville, 2006) permitting measurements in the

temperature interval of 700-1200 K and the viscosity range of 10^8-10^{12} Pa·s. Samples used for the measurements were glass cylinders of 5-7 mm in diameter and 10-15 mm in length with two polished parallel faces. The cylinders were held in a furnace at 600-800 °C for 1 day to remove internal stress before the measurements. To ensure minimal temperature gradient during the measurements a silver cylinder was placed around the sample. This allowed reducing the gradient between the top and the bottom parts of the sample to less than 0.3 K. The thermal gradients along the sample were checked using two Pt–PtRh10% thermocouples. The reported viscosity values at one temperature are the result of an average of 20-40 measurements at different applied stresses. The viscosity uncertainty and reproducibility is less than 0.03 log units with this technique (Neuville, 2006).

Micro-penetration: Glass spheres obtained using the levitation device were too small to use the creep apparatus. Therefore, the viscosity measurements were performed on a homemade micro-indenter. The samples were polished to obtain two parallel faces at least 1 mm in diameter. These surfaces were polished using SiC paper and diamond suspension (1/4-micron particle size). The apparatus is a depth-sensing indentation device, permitting viscosity measurements between 293 and 1373 K with a thermal gradient of ±1 K. The method used to measure the load/penetration and to determine the viscosity from the indentation creep tests is described elsewhere (Bernard et al., 2010; Gueguen et al., 2011). The indenter used was a sphere made of silicon carbide of 2 mm in diameter. The penetration depth has never exceeded 50 µm. The viscosity uncertainty of this method is 0.1 log units.

2.3 DTA measurements

Glass transition temperatures (T_g) of two samples – SA10.45 and SA20.40 – were measured using Setaram® L96 Evo TGA-DTA/DSC apparatus in DTA mode with the heating rate of 5 K/min. T_g was determined as an inflection point of the heat flow curve and a correction of 22 K was then applied to the values to have T_g comparable to those obtained from the viscosity curves at $\log\eta = 12$ Pa·s. This correction value was calibrated by measuring samples with known glass transition temperatures under the same conditions.

2.4 Raman spectroscopy

Unpolarized Raman spectra were recorded at room temperature using a T64000 Jobin-Yvon® triple Raman spectrometer equipped with a confocal system, a 1024 Charge-Coupled Detector cooled by liquid nitrogen and an Olympus® microscope. A Coherent® 70-C5 argon laser with a wavelength of 488.01 nm was used as the excitation source. All spectra were acquired between 20 and 1400 cm^{-1} with acquisition time of 300 s and with 3 repetitions. Before the deconvolution of the

high-frequency region, all spectra were corrected for temperature and excitation line effects using the method of Long (Long, 1977; Neuville and Mysen, 1996). Corrected spectra were normalized to the peak of maximum intensity and then the high-frequency region of the spectra was deconvoluted. All parameters, such as band's frequency, width and intensity were not constrained during the deconvolution procedure.

2.5 Nuclear magnetic resonance spectroscopy

^{27}Al NMR experiments were performed on an Avance III Bruker 850 MHz (20.0 T) spectrometer working at an ^{27}Al frequency of 195.5 MHz. Chemical shifts for ^{27}Al are referenced to a 1 M aqueous $Al(NO_3)_3$ solution. Magic Angle Spinning (MAS) experiments were performed at a spinning speed of 30 kHz in aluminium-free zirconia rotors of 2.5 mm diameter. All spectra were obtained using a single-pulse ("Bloch-decay") sequence using a radio-frequency field ν_{rf} = 62.5 kHz and applying a pulse of 0.4 µs (i.e. less than π/18 to ensure quantitative irradiation). Four thousand scans were accumulated for each composition with a recycling time of 0.15 s (spin-lattice relaxation times found in the range 1-5 s), using a spectral window of 2 MHz to avoid folding of the spinning-sideband's manifold. The decomposition of the spectra was obtained using the dmfit software (Massiot et al., 2002), taking into account the spinning sidebands of the external transitions. This allows extracting the populations of the various components appearing on the central transition, their mean isotropic chemical shifts δ_{iso}, their distributions of isotropic chemical shift $\Delta\delta_{iso}$ and their mean quadrupolar coupling constants C_Q within the framework of the so-called "Czjzek" or "GIM" model (Le Caer and Brand, 1998).

2.6 X-ray absorption spectroscopy

X-ray absorption experiments at the Sr K-edge (16105 eV) were performed at the DIFFABS beamline at the SOLEIL synchrotron (Gif-sur-Yvette, France). This storage ring has energy of 2.75 GeV and was operating in a top up mode with an average electron current of 450 mA. The beamline optics consist of a double Si[111] crystal monochromator surrounded by 2 rhodium coated mirrors. The X-ray beam is focused onto the sample horizontally and vertically by bending the second crystal and the second mirror respectively. The final beam size at the sample position was about 300 µm (H) x 250 µm (V). The actual energy of the monochromator was calibrated at the Y K-edge (17038 eV) using an yttrium calibration foil. The experiments were performed in a transmission mode. The incident and transmitted intensity were measured with two ionization chambers operating with a nitrogen flux at atmospheric pressure as absorbing gas. All studied samples were crushed to a fine powder. An appropriate quantity to provide an absorbance jump of 1 at the edge was ground with boron nitride (BN) and pressed into pellets with a thickness of about 250 µm. Each spectrum is an

average of 3 measurements performed with a step of 2 eV which was reduced to 1 eV around the absorption edge. The data reduction was performed using the Athena software (Ravel and Newville, 2005).

3. RESULTS

3.1 Viscosity

The viscosity measurements are presented in Table 2 and plotted in Figure 1 as a function of reciprocal temperature. When considering the two extreme compositions – SA75.12 and SA26.37, a difference of about 15 K at constant viscosity of 10^{12} Pa·s and almost an order of magnitude in the viscosities at T = 1169 K (T_g of SA75.12) are observed. Low-temperature viscosity data were fitted by using the Vogel–Fulcher–Tammann-Hesse (VFTH) equation:

$$log\eta = A + \frac{B}{T-T_1}, \quad (1)$$

where η is the viscosity in Pa·s, T is the temperature in K and A, B, T_1 are adjustable parameters given in Table 3. The glass transition temperatures T_g were obtained from the fitting of the experimental data and are summarized in Table 3 and shown in Figure 2 (along with the data derived from DTA measurements). The inset in Figure 1 represents the viscosity of the melts plotted as a function of T_g/T and illustrates the evolution of the melts' fragilities (m) (Angell, 1991), i.e. the gradient of the viscosity curve at the glass transition temperature on a reduced temperature scale (Plazek and Ngai, 1991; Böhmer and Angell, 1992). It can be calculated by the following equation:

$$m = \left.\frac{d(log_{10}\eta)}{d(\frac{T_g}{T})}\right|_{T=T_g} = \frac{B}{T_g(1-T_1/T_g)^2}, \quad (2)$$

where B and T_1 are recovered from the equation (1). The calculated fragilities are listed in the Table 3.

From the inset in Figure 1 one can see that the melts become more fragile upon decreasing the silica content. The viscosity of melts can also be connected to their entropy of configuration through the Adam and Gibbs theory (Adam and Gibbs, 1965; Urbain, 1974; Richet, 1984; Scherer, 1984; Neuville and Richet, 1991):

$$log\eta = A_e + \frac{B_e}{T \cdot S^{conf}(T)}, \quad (3)$$

where η is the viscosity in Pa·s, T is the temperature in K, A_e is a pre-exponential factor, B_e is a constant proportional to the potential barrier opposed to the cooperative rearrangement of the liquid's structure and $S^{conf}(T)$ is the melt's configurational entropy. $S^{conf}(T)$ can be calculated from the following equation:

$$S^{conf}(T) = S^{conf}(T_g) + \int_{T_g}^{T} C_p^{conf}/TdT, \quad (4)$$

where $S^{conf}(T_g)$ is the configurational entropy of the melt at T_g, C_p^{conf} is the configurational heat capacity calculated as a difference of heat capacities of the glass at T_g, $C_{p,g}(T_g)$, and the heat capacity of the liquid, $C_{p,l}$, determined from Richet and Botinga (1985). Partial molar heat capacities of SiO_2 and Al_2O_3 for the calculations of $C_{p,g}(T_g)$ were taken from Richet (1987) and the value of partial molar heat capacity of crystalline SrO was taken from Robie et al. (1978), following previous calculations by Neuville (2006). Combining equations (3) and (4), parameters such as $S^{conf}(T_g)$, A_e and B_e can be estimated (Table 3).

In Figure 2 the glass transition temperatures T_g of the studied glasses derived from viscosity and DTA measurements are plotted as a function of silica content. T_g decreases rapidly with the addition of even a small quantities of $SrAl_2O_4$ to the silica glass. After this, a slight decrease in T_g is observed upon changing the composition from SA75.12 to SA42.29. The latter has the minimal T_g and with further addition of $SrAl_2O_4$ the glass transition temperature starts to increase again, similarly to observations made on the tectosilicate join of the CaO-Al_2O_3-SiO_2 system (Neuville et al., 2004b).

3.2 Raman spectroscopy

Figure 3a presents unpolarised raw spectra of SAS glasses. The Raman spectra can be divided into four regions: the Boson region (20-250 cm^{-1}), the low frequency region (250-700 cm^{-1}), the intermediate region (700-850 cm^{-1}), and the high frequency region (850-1300 cm^{-1}).

The boson region (20-250 cm^{-1}). The origin of the boson peak has been attributed to rotational motions of interconnected tetrahedral units (Bucheneau et al., 1986; Hehlen et al., 2000, 2002; Courtens et al., 2001). It becomes more pronounced and shows a shift of approximately 1 cm^{-1} each 10 % of silica added to $SrAl_2O_4$. (Figure 3b). This decrease can be extrapolated up to Sr aluminate and are found in agreement with previous measurements (Licheron et al., 2011). This variation in frequency as a function of composition is found to be a linear combination of that of the pure SiO_2 and $SrAl_2O_4$ compounds.

The low frequency region (250-700 cm^{-1}). In the Raman spectrum of SiO_2 three bands are clearly observed at 600, 490, and 435 cm^{-1}. These bands are well known and attributed to 3-, 4- and higher-membered rings of SiO_4 tetrahedra, respectively (Sharma et al., 1981; Galeener, 1982a,b; Galeener et al., 1984; McMillan et al., 1994; Pasquarello and Car, 1998; Umari and Pasquarello, 2002; Rahmani et al., 2003; Kalampounias et al., 2006). The band at 500 cm^{-1} decreases in intensity and shifts strongly to a higher frequency when SiO_2 is substituted by $SrAl_2O_4$ and becomes a shoulder for the compositions with SiO_2 content less than 42 mol%. A new band appears at 560 cm^{-1}, increases in intensity and moves a little to lower frequency upon decreasing silica content. It is observed as a shoulder for the compositions with SiO_2 content above 42 mol%. These two bands are usually

assigned to vibrations of three- (~ 560 cm^{-1}) and four-membered (~ 500 cm^{-1}) rings of tetrahedra present in the aluminosilicate network (McMillan, 1984).

The intermediate frequency region (700-850 cm^{-1}). A band at 800 cm^{-1} is observed for SiO_2. This band is usually attributed to the threefold degenerate "rigid cage" vibrational mode of TO_2 units (Galeener, 1979), to the motion of the Si atom in its oxygen cage (Mysen et al., 1982) or to Si–O stretching involving oxygen motions in the Si–O–Si plane (McMillan et al., 1994). It decreases in intensity rapidly with decreasing silica content and moves to lower frequency. A band appearing in this region again for SA20.40 and more visibly for SA10.45 has a different nature and could possibly be related to a shift of the entire high-frequency envelope to lower frequency under substitution of SiO_2 by $SrAl_2O_4$.

The high frequency region (850-1300 cm^{-1}). For SiO_2 glass in the high frequency region two broad bands are observed. They merge into a single band for SA75.12, and this band becomes narrower and shifts to lower frequency with decreasing silica content, similarly to what has been observed for MAS and CAS tectosilicate glasses (Neuville et al., 2006, 2008a). Several studies pointed out that different peaks are convoluted in this band, arising from the T-O stretching (T = Si, Al) in different Q^n tetrahedral units, where n is the number of bridging oxygens and Q is the four-fold coordinated cation (McMillan, 1984; Mysen, 1999).

Spectra deconvolution. Before treating the high frequency region, the Raman spectra of the SAS glasses were corrected for temperature and excitation line effects (Long, 1977). The spectra were then simulated following Mysen (1999) using three Gaussians bands as proposed by several authors (Seifert et al., 1982; Neuville and Mysen, 1996 (Figure 4a)). These three bands have been observed in silica glass as well as in alkali and alkaline earth tectosilicate glasses (Mysen et al, 1982; Neuville and Mysen, 1996; Neuville et al., 2004a, 2008a; Le Losq et al., 2014). Bands' parameters are reported in Table 4 and the bands' frequencies are plotted as a function of silica content in Figure 4b together with data for sodium, magnesium and calcium tectosilicates. All three bands shift to lower frequencies with decreasing silica content, changing from 990, 1100 and 1182 cm^{-1} for SA75.12 to 814, 926 and 1007 cm^{-1} for SA10.45. The two higher frequency bands have been attributed to two Q^4 units in two different structural environment presenting a T-O-T angle difference of about 5-10° (Seifert et al., 1982). The band at the highest frequency, called $Q^{4,I}$, arises from Q^4 units with a larger T-O-T angles than the band at lower frequency, called $Q^{4,II}$, having a smaller T-O-T angles. The lowest frequency band has been reported in spectra of vitreous silica, alkali and alkaline earth silicate and aluminosilicate glasses and melts (Mysen et al., 1982; McMillan, 1984; Neuville and Mysen, 1996). It has been suggested by Le Losq and Neuville, (2013) that this band can arise from a stretching T_{2s} vibrational mode of TO_4 tetrahedra.

3.3 NMR spectroscopy

The ^{27}Al quantitative 1 pulse MAS NMR spectra of the investigated SAS glasses are shown in Figure 5. The NMR bands consist of the main contribution which maximum shifts from approximately 55 to 78 ppm with decreasing SiO_2 content, positions characteristic of four-fold coordinated aluminium, $Al^{[4]}$. A small shoulder around 30-45 ppm is also visible for almost all compositions and is ascribed to the presence of aluminium in five-fold coordination, $Al^{[5]}$ (MacKenzie and Smith, 2002; Massiot et al., 2002; Neuville et al., 2004a) and similar contributions have also been observed for MAS and CAS glasses (Neuville et al. 2004a, 2006, 2007, 2008a). These spectra are very satisfactorily simulated using fully random distribution of quadrupolar and isotropic chemical shift interactions as expressed within the GIM model (Le Caer and Brand, 1998). The retrieve average isotropic chemical shift δ_{iso}, mean quadrupolar coupling constant C_Q and population of each site are given in Table 5. The average isotropic chemical shift, δ_{iso}, for $Al^{[4]}$ increases linearly with increasing SiO_2 content (Figure 6a) in a manner very similar to the one observed for the MAS and CAS systems on the same joins, independent of the XO/Al_2O_3 ratio (X = Sr, Ca, or Mg). This suggests similar chemical AlO_4 environments in these three systems, the δ_{iso} being mainly controlled by the progressive substitution of Al by Si in the first coordination sphere of Al (Florian et al., 2012). Less precisely defined because of much lower intensity, the average isotropic chemical shift of the $Al^{[5]}$ species also follows an overall linear decrease with increasing SiO_2 content, in agreement with previous observations for Mg- and Ca-based systems. The average quadrupolar coupling constant C_Q for $Al^{[4]}$ is found between 7.0 MHz and 8.1 MHz, i.e. close to typical values found for Ca-based glasses (5.9 MHz to 9.3 MHz; Neuville et al., 2006) and slightly below those obtained on Mg-based systems (7.6 MHz to 10.0 MHz; Neuville et al., 2008a).

The maximum in $Al^{[5]}$ population for SAS glasses (see Figure 6b) corresponds to 4.5 % and is found for the compositions in the middle of the ternary system, i.e. close to the ones found in MAS and CAS systems (Neuville et al., 2006, 2008a).

3.4 X-ray absorption spectroscopy at Sr K-edge

Normalized spectra of SAS glasses together with a crystalline standard (strontianite, $SrCO_3$) are presented in Figure 7. The position of the white line is around 16105 eV for all compositions investigated and for the crystalline standard, which confirms that strontium is in the oxidation state +2. The XANES Sr K-edge spectra of all glasses are almost similar to that of the strontianite. This may imply that Sr in SAS glasses has a coordination number similar to the one found in $SrCO_3$. Coordination number has been reported by different authors to be 9 for strontianite (De Villeirs, 1971; Antao and Hassan, 2009; Ye et al. 2012). This value is higher than those proposed by McKeown et al. (2003) for Sr borosilicates and also higher than the 6-7 coordination number found for Ca

aluminosilicate glasses with analogous compositions (Neuville et al., 2004b). A precise data analysis is underway, in order to confirm these fingerprint observations.

4. DISCUSSION

4.1 Structural changes along the SiO_2-$SrAl_2O_4$ join

The knowledge of the aluminosilicate glasses and melts structure is a key to understand the variation of macroscopic properties such as viscosity and glass transition temperature. This key may be lifted by coupling NMR and XANES studies, giving information about the short-range order, coordination number and speciation, and Raman spectroscopy which brings knowledge about the ring organization and polymerization of the glass and melt. Finally, both approaches provide information about the glasses and melts' structure and can be directly correlated to the viscosity through the configurational entropy variation as shown by Neuville and Mysen (1996).

Common wisdom dictates that the tectosilicate glass network at both high and low silica content is fully polymerized and consists solely of corner sharing tetrahedral units TO_4 (T = Si, Al). In other words, in all compositions being on the charge compensation line, Al and Si are expected to stay as Q^4 species, i.e. only a very small amount of NBOs are expected to present (Farnan et al., 1992; Allwardt and Stebbins, 2004; Thompson and Stebbins, 2012). SiO_2 glass is the simplest model of a fully polymerized glass structure and can be approximated by using the central-force model (Sen and Thorpe, 1977; Galeener, 1979), used by Seifert et al. (1982) to propose that SiO_2 is composed of two different coexisting structures with different inter-tetrahedral angles: $Q^{4,I}$, and $Q^{4,II}$. These two interconnected structures in vitreous SiO_2 have subsequently been found in alkali and alkaline earth aluminosilicates by a range of Raman studies (Seifert et al., 1982; Neuville and Mysen, 1996; Neuville et al., 2004a,b, 2006, 2008a; Le Losq and Neuville, 2013). It should nevertheless be noted that no other techniques have yet evidenced such a bimodal distribution of Si-O-Si inter-tetrahedral angles.

For glasses along the SiO_2-$SrAl_2O_4$ join, the Raman spectra exhibit changes in the low and high frequency regions. In the silica's spectrum in the low frequency region signals from 3-, 4- and higher-membered rings are observed (with a significant fraction of high-membered rings; see Figure 3a). With introduction of $SrAl_2O_4$ (e.g., SA75.12) the fraction of high-membered rings decreases and further addition of $SrAl_2O_4$ favours formation of low-membered rings (e.g., SA10.45). In the high frequency regions Raman spectra exhibit a continuous shift of the band frequencies as a function of the Al/(Al+Si) ratio as already seen in the NAS, MAS and CAS systems. The high frequency envelope of the Raman spectra of glasses along this join was simulated (Figure 4a) using three bands associated with two Q^4 units and the T_{2S} band (Seifert et al., 1982; Neuville and Mysen, 1996; Neuville et al., 2004a; Le Losq et al., 2014; Neuville et al., 2014). In Figure 4b, the wavenumbers of

the three bands after deconvolution are plotted as a function of SiO_2 content showing no evidence for the appearance of new bands with decreasing silica content. The negative frequency change with increasing Al_2O_3 content is consistent with aluminium substitution for Si in these units (Neuville and Mysen, 1996; Mysen, 1999). This substitution produces a linear shift in the Raman frequency (Neuville and Mysen, 1996; Neuville et al., 2006, 2008a). The Raman spectra of SAS glasses follow a similar trend as the one observed for the glasses in CAS (Seifert et al., 1982; Neuville et al., 2006), MAS (Neuville et al., 2008a) and NAS (Seifert et al., 1982; Neuville and Mysen, 1996) systems. This is in good agreement with Merzbacher and White (1991) who have shown that the substitution of alkaline earth element produces a very small effect on the Raman spectra. This indicates that, on the tectosilicate join, Si/Al substitution has larger influence on the aluminosilicate network than the nature of a cation, which plays the role of a charge compensator. Nevertheless, Raman spectroscopy probing the medium range order is not able to investigate the short range order and detect minor species such as, for example, aluminium in the five-fold coordination state (Neuville et al., 2004a, 2006, 2008a). This is the reason why NMR spectroscopy was used to investigate aluminium environment.

^{27}Al NMR data indicate that the majority (at least 95%) of aluminium atoms are in four-fold coordination. Figure 6a shows significant changes in δ_{iso} for $Al^{[4]}$ sites as a function of silica content, where, in agreement with previous values for MAS and CAS systems (Neuville et al., 2004a, 2006, 2008a), the δ_{iso} goes from 62 up to 79 ppm respectively for 76 and 0 mol% of SiO_2. This linear decrease of δ_{iso} results from a purely random substitution of Si by Al in the second coordination sphere of aluminium, which produces an approximate -3 ppm shift per substitution (Florian et al, 2012) and is to be related to the bands' shifts also observed in the high frequency regions of the Raman spectra (vide supra). The evolution of the $Al^{[5]}$ population as a function of silica content (Figure 6b) for SAS glasses possesses a maximum (~4.5 % of five-fold aluminium) that is clearly observed between 42 and 50 mol% of SiO_2. This maximum is shifted to lower silica content (33-42 mol%) for the CAS system, while for the MAS system it is difficult to assume the same trend since no data are available in the low-silica region.

In the SAS system, the proportion of $Al^{[5]}$ is lower than that observed in MAS and CAS glasses which is in a good agreement with previous studies on alkali, earth alkaline and rare earth aluminosilicates which show that the increase of the cation field strength directly correlates with an increase of the $Al^{[5]}$ population (Allwardt et al., 2005b; Florian et al., 2007; Iftekhar et al., 2011; Thompson and Stebbins, 2012). In this respect, the SrO-Al_2O_3-SiO_2 system has a behaviour similar to sodium aluminosilicate glasses which have a small to non-detectable amount of high coordinated Al species (Stebbins et al., 1992; Allwardt et al., 2005a,b). Contrarily to MAS and CAS systems, $Al^{[6]}$ is

not detected in SrO-Al_2O_3-SiO_2 glasses apart from a couple of compositions for which it represents less than 0.5 % of the total intensity.

4.2 Influence of structural changes on macroscopic properties

It is well known that the SiO_2 glass network consists only of SiO_4 tetrahedra forming low- and high-membered rings (Figure 3a) hence $S^{conf}(T_g)$ is minimal in this case (Figure 8) and consists of a pure topological contribution (Richet and Neuville, 1992). Under substitution of SiO_2 by $SrAl_2O_4$ the following changes take place. The number of particles in the system increases (two AlO_4^- units for one Sr^{2+} cation), additional structural units (AlO_4, AlO_5) appear in the system and tetrahedral rings start to include not only SiO_4 but also AlO_4. As expected, the fragility (inset of Figure 1) increases with decreasing SiO_2 content. This proves that, when Al goes in tetrahedral position and substitutes Si, it produces Al-O-Al linkages which are weaker than Si-O-Si ones. In agreement with Angell (1991), the increase in fragility also well correlates with the increase in the $C_{p,l}/C_{p,g}$ from 1.1 up to 1.2 where $C_{p,l}$ values were calculated from the partial heat capacity of the liquid from Richet and Bottinga (1985) and $C_{p,g}$ values were calculated from partial heat capacity of the glass for SiO_2 and Al_2O_3 from Richet (1987) and for SrO from Robie et al. (1978). Starting from a pure topological contributions to the configurational entropy (5 J/mol·K for SiO_2 glass), some new topological and chemical contributions are added upon addition of $SrAl_2O_4$ into SiO_2 leading to an increase of $S^{conf}(T_g)$ (Figure 8) and to a rapid drop in T_g under introduction of small quantities of $SrAl_2O_4$ into SiO_4-based network. Going from 75 to 42 mol% of silica T_g decreases gradually (Figure 2) as a consequence of an increasing melts fragility, increasing disorder in the system and increasing fraction of AlO_5 (reaching a maximum of 4.5 % at 42-50 mol% of SiO_2; see Figure 6b). Below 42 mol% of silica the melts' fragility continues to increase while the fraction of low-membered rings prevails and the AlO_5 content decreases down to 1.4 %. $S^{conf}(T_g)$ seems to reach a plateau around 21 J/mol·K in this region (Figure 8) and it is likely that different contributions to the configurational entropy start to compensate each other in this low-silica content region. For example, the number of particles continues to increase with addition of $SrAl_2O_4$, but at the same time the number of different structural units decreases (less SiO_4 and AlO_5). Considering the lack of the viscosity data (and hence values of $S^{conf}(T_g)$) for the compositions SA20.40, SA10.45 we can only assume that the observed increase in T_g with further decrease in SiO_2 content is due to a progressive ordering of the system.

A similar behaviour has been already observed in the CaO-Al_2O_3-SiO_2 system, where the viscosities and glass transition temperatures first decrease with SiO_2 content decreasing down to 30 mol% and then increase with further decreasing SiO_2 (Neuville, 1992; Neuville et al., 2004b). It is worth noticing that the maximum in $Al^{[5]}$ content (Figure 6b), observed for the composition SA42.29, corresponds to the minimum in T_g (Figure 2). The same trend has been seen for the Ca tectosilicates

where a maximum in $Al^{[5]}$ and a minimum in T_g are observed for the composition CA33.33 (Neuville et al., 2004a,b, 2006). Thus, five-fold coordinated Al can be seen as having a similar role as $Si^{[5]}$ species in promoting the viscous flow (Farnan and Stebbins, 1994). Such a participation of the AlO_5 units in the network mobility has been proposed by Poe et al. (1994) for aluminate melts and more recently by Le Losq et al. (2014) for aluminosilicate melts. In other words, since in both systems, SAS and CAS, the minimum in T_g matches with the maximum in AlO_5 content we can conclude that minor species such as AlO_5 should significantly influence the transport mechanisms for the tectosilicate compositions (Neuville et al., 2008b).

5. CONCLUSION

Spectroscopic investigations of SrO-Al_2O_3-SiO_2 glasses were made using Raman, NMR and X-ray absorption spectroscopy in order to obtain information on short and medium range order on glass structure and correlate those to viscosity measurements close to the glass transition temperature. All these experiments give a better knowledge on this ternary system, in particular:

- $Al^{[5]}$ is present in all studied glasses, though in quantities less that for Mg and Ca aluminosilicates with similar compositions. A maximum of approximately 4.5 % of five-fold aluminium environments has been found for the compositions around 40-50 mol% of SiO_2.
- X-ray absorption spectroscopy indicates that the first coordination shell of strontium in tectosilicate glasses is close to that found in strontianite. This suggests a coordination number of Sr close to 9, which is higher than that of Mg and Ca for analogous compositions in MAS and CAS systems. A detailed analysis is underway and should allow us to shed light on Sr coordination in these compounds.
- Aluminium randomly replaces silicon in tetrahedral units when $SrAl_2O_4$ added to silica leading to a linear shift of the high frequency Raman bands as well as of the average chemical shifts of $Al^{[4]}$ and $Al^{[5]}$. Such linear trends and negative correlation between ^{27}Al NMR and Raman has been previously observed for Mg and Ca aluminosilicates.
- Viscosity and DTA measurements show the presence of a minimum in T_g for the composition with 42 mol% of silica. With further addition of $SrAl_2O_4$ T_g increases slightly. Similar observations have been made for Ca tectosilicates. Calculated values of $S^{conf}(T_g)$ increases gradually while SiO_2 content decreases pointing to an increase of disorder in the system while replacing Si by Al in the glass network.

Acknowledgments

The authors would like to thank Lilian Latapie for help in viscosity measurements. Franck Fayon is acknowledged for helping with NMR experiments. Thanks are due to the OXYMORE funding from Île-de-France region for supporting purchase a Multi HT96 LINE TGA-DTA/DSC Setaram®. This research was conducted under funding from ANR DyStrAS project (ANR-13-BS08-0012). We also acknowledge an anonymous reviewer whose explicit comments helped to improve the quality of the paper.

References

Adam, G., Gibbs, J.H., 1965. On the Temperature Dependence of Cooperative Relaxation Properties in Glass-Forming Liquids. J. Chem. Phys. 43, 139–146. doi:10.1063/1.1696442

Abel, B.M., Morgan, J.M., Mauro, J.C., Smedskjaer, M.M., 2013. Liquidus Temperature of SrO-Al_2O_3-SiO_2 Glass-Forming Compositions. Int. J. Appl. Glas. Sci. 4, 225–230. doi:10.1111/ijag.12017

Allwardt, J.R., Stebbins, J.F., 2004. Ca-Mg and K-Mg mixing around non-bridging O atoms in silicate glasses: An investigation using ^{17}O MAS and 3QMAS NMR. Am. Mineral. 89, 777–784. doi:10.2138/am-2004-5-611

Allwardt, J.R., Poe, B.T., Stebbins, J.F., 2005a. The effect of fictive temperature on Al coordination in high-pressure (10 GPa) sodium aluminosilicate glasses. Am. Mineral. 90, 1453–1457. doi:10.2138/am.2005.1736

Allwardt, J.R., Stebbins, J.F., Schmidt, B.C., Frost, D.J., Withers, A.C., Hirschmann, M.M., 2005b. Aluminum coordination and the densification of high-pressure aluminosilicate glasses. Am. Mineral. 90, 1218–1222. doi:10.2138/am.2005.1836

Al Saghir, K., Chenu, S., Veron, E., Fayon, F., Suchomel, M., Genevois, C., Porcher, F., Matzen, G., Massiot, D., Allix, M., 2015. Transparency through structural disorder: A new concept for innovative transparent ceramics. Chem. Mater. 27, 508–514. doi:10.1021/cm5037106

Angell, C.A., 1991. Relaxation in liquids, polymers and plastic crystals - strong/fragile patterns and problems. J. Non. Cryst. Solids 131-133, 13–31. doi:10.1016/0022-3093(91)90266-9

Antao, M.S., Hassan, I., 2009. The orthorhombic structure of $CaCO_3$, $SrCO_3$, $PbCO_3$ and $BaCO_3$: Linear structural trends. Can. Mineral. 47, 1245–1255. doi:10.3749/canmin.47.5.1245

Bansal, N.P., 1998. Solid State Synthesis and Properties of Monoclinic Celsian. J. Mater. Sci. 33, 4711–4715. doi:10.1023/A:1004484903436

Beall, G.H., 2009. Refractory glass-ceramics based on alkaline earth aluminosilicates. J. Eur. Ceram. Soc. 29, 1211–1219. doi:10.1016/j.jeurceramsoc.2008.08.010

Bernard, C., Keryvin, V., Sangleboeuf, J.-C., Rouxel, T., 2010. Indentation creep of window glass around glass transition. Mech. Mater. 42, 196–206. doi:10.1016/j.mechmat.2009.11.008

Bockris, J.O., MacKenzie, J.D., Kitchener, J.A., 1955. Viscous flow in silica and binary liquid silicates. Trans. Faraday Soc. 51, 1734–1748. doi:10.1039/TF9555101734

Böhmer, R., Angell, C.A., 1992. Correlations of the nonexponentiality and state dependence of mechanical relaxations with bond connectivity in Ge-As-Se supercooled liquids. Phys. Rev. B 45, 10091–10094. doi:10.1103/PhysRevB.45.10091

Bruckner, R., 1970. Properties and structure of vitreous silica. I. J. Non. Cryst. Solids 5, 123–175. doi:10.1016/0022-3093(70)90190-0

Buchenau, U., Prager, M., Nucker, N., Dianoux, A.J., Ahmad, N., Phillips, W.A., 1986. Low-frequency modes in vitreous silica. Phys. Rev. B 34, 5665–5673. doi:10.1103/PhysRevB.34.5665

Capo, R.C., Stewart, B.W., Chadwick, O.A., 1998. Strontium isotopes as tracers of ecosystem processes: theory and methods. Geoderma 82, 197–225. doi:10.1016/S0016-7061(97)00102-X

Chiari, G., Calleri, M., Bruno, E., Ribbe, P.H., 1975. The structure of partially disordered, synthetic strontium feldspar. Am. Mineral. 60, 111–119.

Courtens, E., Foret, M., Hehlen, B., Vacher, R., 2001. Vibrational modes of glasses. Solid State Commun. 117, 187–200. doi:10.1016/S0038-1098(00)00434-8

Creux, S., Bouchet-Fabre, B., Gaskell, P.H., 1995. Anomalous wide angle X-ray scattering study of strontium silicate and aluminosilicate glasses. J. Non. Cryst. Solids 192-193, 360–363. doi:10.1016/0022-3093(95)00377-0

DePaolo, D.J., 1981. Trace element and isotopic effects of combined wallrock assimilation and fractional crystallization. Earth Planet. Sci. Lett. 53, 189–202. doi:10.1016/0012-821X(81)90153-9

De Villiers, J.P.R., 1971. Crystal structures of aragonite , strontianite , and witherite. Am. Mineral. 56, 758–767.

Drewitt, J.W.E., Hennet, L., Zeidler, A., Jahn, S., Salmon, P.S., Neuville, D.R., Fischer, H.E., 2012. Structural transformations on vitrification in the fragile glass-forming system $CaAl_2O_4$. Phys. Rev. Lett. 109, 235501. doi:10.1103/PhysRevLett.109.235501

Farnan, I., Stebbins, J.F., 1994. The nature of the glass transition in a silica-rich oxide melt. Science . 265, 1206–1209. doi:10.1126/science.265.5176.1206

Farnan, I., Grandinetti, P.J., Baltisberger, J.H., Stebbins, J.F., Werner, U., Eastman, M.A., Pines, A., 1992. Quantification of the disorder in network-modified silicate glasses. Nature 358, 31–35. doi:10.1038/358031a0

Faure, G., Powell, J.L., 1972. Strontium Isotope Geology. Springer Berlin Heidelberg, Berlin, Heidelberg. doi:10.1007/978-3-642-65367-4

Florian, P., Sadiki, N., Massiot, D., Coutures, J.P., 2007. ^{27}Al NMR Study of the Structure of Lanthanum- and Yttrium-Based Aluminosilicate Glasses and Melts. J. Phys. Chem. B 111, 9747–9757. doi:10.1021/jp072061q

Florian, P., Veron, E., Green, T.F.G., Yates, J.R., Massiot, D., 2012. Elucidation of the Al/Si Ordering in Gehlenite $Ca_2Al_2SiO_7$ by Combined ^{29}Si and ^{27}Al NMR Spectroscopy/Quantum Chemical Calculations. Chem. Mater. 24, 4068–4079. doi:10.1021/cm3016935

Frantz, J.D., Mysen, B.O., 1995. Raman spectra and structure of $BaO-SiO_2$, $SrO-SiO_2$ and $CaO-SiO_2$ melts to 1600°C. Chem. Geol. 121, 155–176. doi:10.1016/0009-2541(94)00127-T

Fukumi, K., Hayakawa, J., Komiyama, T., 1990. Intensity of Raman band in silicate glasses. J. Non. Cryst. Solids 119, 297–302. doi:10.1016/0022-3093(90)90302-3

Furukawa, T., Fox, K., White, W., 1981. Raman spectroscopic investigation of the structure of silicate glasses. III. Raman intensities and structural units in sodium silicate glasses. J. Chem. Phys. 75, 3226-3237. doi: 10.1063/1.442472

Galeener, F.L., 1979. Band limits and the vibrational spectra of tetrahedral glasses. Phys. Rev. B 19, 4292–4297. doi:10.1103/PhysRevB.19.4292

Galeener, F.L., 1982a. Planar rings in vitreous silica. J. Non. Cryst. Solids 49, 53–62. doi:10.1016/0022-3093(82)90108-9

Galeener, F.L., 1982b. Planar rings in glasses. Solid State Commun. 44, 1037–1040. doi:10.1016/0038-1098(82)90329-5

Galeener, F.L., Barrio, R.A., Martinez, E., Elliott, R.J., 1984. Vibrational Decoupling of Rings in Amorphous Solids. Phys. Rev. Lett. 53, 2429–2432. doi:10.1103/PhysRevLett.53.2429

Gueguen, Y., Rouxel, T., Gadaud, P., Bernard, C., Keryvin, V., Sangleboeuf, J.C., 2011. High-temperature elasticity and viscosity of Ge_xSe_{1-x} glasses in the transition range. Phys. Rev. B - Condens. Matter Mater. Phys. 84, 1–10. doi:10.1103/PhysRevB.84.064201

Hehlen, B., Courtens, E., Vacher, R., Yamanaka, A., Kataoka, M., Inoue, K., 2000. Hyper-Raman scattering observation of the boson peak in vitreous silica. Phys. Rev. Lett. 84, 5355–8. doi:10.1103/PhysRevLett

Hehlen, B., Courtens, E., Yamanaka, A., Inoue, K., 2002. Nature of the Boson peak of silica glasses from hyper-Raman scattering. J. Non. Cryst. Solids 307-310, 87–91. doi:10.1016/S0022-3093(02)01444-8

Hennet, L., Pozdnyakova, I., Bytchkov, A., Cristiglio, V., Palleau, P., Fischer, H.E., Cuello, G.J., Johnson, M., Melin, P., Zanghi, D., Brassamin, S., Brun, J.F., Price, D.L., Saboungi, M.L., 2006. Levitation apparatus for neutron diffraction investigations on high temperature liquids. Rev. Sci. Instrum. 77. doi:10.1063/1.2200756

Hennet, L., Drewitt, J.W.E., Neuville, D.R., Cristiglio, V., Kozaily, J., Brassamin, S., Zanghi, D., Fischer, H.E., 2016. Neutron diffraction of calcium aluminosilicate glasses and melts. J. Non. Cryst. Solids 1–6. doi:10.1016/j.jnoncrysol.2016.05.018

Hyatt, M.J., Bansal, N.P., 1996. Crystal growth kinetics in $BaOAl_2O_32SiO_2$ and $SrOAl_2O_32SiO_2$ glasses. J. Mater. Sci. 31, 172–184. doi:10.1007/BF00355142

Iftekhar, S., Grins, J., Gunawidjaja, P.N., Edén, M., 2011. Glass Formation and Structure-Property-Composition Relations of the $RE_2O_3-Al_2O_3-SiO_2$ (RE = La, Y, Lu, Sc) Systems. J. Am. Ceram. Soc. 94, 2429–2435. doi:10.1111/j.1551-2916.2011.04548.x

Jakse, N., Bouhadja, M., Kozaily, J., Drewitt, J.W.E., Hennet, L., Neuville, D.R., Fischer, H.E., Cristiglio, V., Pasturel, A., 2012. Interplay between non-bridging oxygen, triclusters, and fivefold Al coordination in low silica content calcium aluminosilicate melts. Appl. Phys. Lett. 101. doi:10.1063/1.4766920

Kalampounias, A.G., Yannopoulos, S.N., Papatheodorou, G.N., 2006. Temperature- induced structural changes in glassy, supercooled, and molten silica from 77 to 2150 K. J. Chem. Phys. 124. doi:10.1063/1.213687

Kanehashi, K., Stebbins, J.F., 2007. In situ high temperature ^{27}Al NMR study of structure and dynamics in a calcium aluminosilicate glass and melt. J. Non. Cryst. Solids 353, 4001–4010. doi:10.1016/j.jnoncrysol.2007.06.030

Le Caër, G., Brand, R.A., 1999. General models for the distributions of electric field gradients in disordered solids. J. Phys. Condens. Matter 10, 10715–10774. doi:10.1088/0953-8984/10/47/020

Le Losq, C., Neuville, D.R., 2013. Effect of the Na/K mixing on the structure and the rheology of tectosilicate silica-rich melts. Chem. Geol. 346, 57–71. doi:10.1016/j.chemgeo.2012.09.009

Le Losq, C., Neuville, D.R., Florian, P., Henderson, G.S., Massiot, D., 2014. The role of Al^{3+} on rheology and structural changes in sodium silicate and aluminosilicate glasses and melts. Geochim. Cosmochim. Acta 126, 495–517. doi:10.1016/j.gca.2013.11.010

Le Losq, C, Neuville, D.R., Florian, P., Massiot, D., Zhou, Z., Chen, W., Greaves, N., 2016. Percolation channels: a universal idea to describe the atomic structure of glasses and melts. Nat. comm. (in preparation).

Licheron, M., Montouillout, V., Millot, F., Neuville, D.R., 2011. Raman and ^{27}Al NMR structure investigations of aluminate glasses: $(1-x)Al_2O_3 - x$ MO, with M = Ca, Sr, Ba and $0.5<x<0.75$). J. Non. Cryst. Solids 357, 2796–2801. doi:10.1016/j.jnoncrysol.2011.03.001

Long, D.A., 1977. Raman Spectroscopy. McGraw Hill, New York.

MacKenzie, K.J.D., Smith, M.E., 2002. Multinuclear Solid StateNMR of Inorganic Materials. Pergamon.

Magaritz, M., Hofmann, A.W., 1978. Diffusion of Sr, Ba and Na in obsidian. Geochim. Cosmochim. Acta 42, 595–605. doi:10.1016/0016-7037(78)90004-2

Massiot, D., Fayon, F., Capron, M., King, I., Le Calvé, S., Alonso, B., Durand, J.O., Bujoli, B., Gan, Z., Hoatson, G., 2002. Modelling one- and two-dimensional solid-state NMR spectra. Magn. Reson. Chem. 40, 70–76. doi:10.1002/mrc.984

McKeown, D.A., Kot, W.K., Gan, H., Pegg, I.L., 2003. X-ray absorption studies of local strontium environments in borosilicate waste glasses. J. Non. Cryst. Solids 317, 290–300. doi:10.1016/S0022-3093(03)00482-4

McMillan, P., 1984. Structural studies of silicate glasses and melts-applications and limitations of Raman spectroscopy. Am. Mineral. 69, 622–644.

McMillan, P.F., Poe, B.T., Gillet, P.H., Reynard, B., 1994. A study of SiO_2 glass and supercooled liquid to 1950 K via high-temperature Raman spectroscopy. Geochim. Cosmochim. Acta 58, 3653–3664. doi:10.1016/0016-7037(94)90156-2

Merzbacher, C.I., White, W.B., 1991. The structure of alkaline earth aluminosilicate glasses as determined by vibrational spectroscopy. J. Non. Cryst. Solids 130, 18–34. doi:10.1016/0022-3093(91)90152-V

Moorbath, S., Allaart, J.H., Bridgwater, D., McGregor, V.R., 1977. Rb–Sr ages of early Archaean supracrustal rocks and Amîtsoq gneisses at Isua. Nature 270, 43–45. doi:10.1038/270043a0

Mysen, B.O., 1990. Role of Al in depolymerized, peralkaline aluminosilicate melts in the systems Li_2O-Al_2O_3-SiO_2, Na_2O-Al_2O_3-SiO_2, and K_2O-Al_2O_3-SiO_2. Am. Mineral. 75, 120–134.

Mysen, B.O., 1999. Structure and properties of magmatic liquids: From haplobasalt to haploandesite. Geochim. Cosmochim. Acta 63, 95–112. doi:10.1016/S0016-7037(98)00273-7

Mysen, B.O., Frantz, J.D., 1993. Structure and properties of alkali silicate melts at magmatic temperatures. Eur. J. Mineral. 5, 393–407. doi:10.1127/ejm/5/3/0393

Mysen, B.O., Frantz, J.D., 1994. Silicate melts at magmatic temperatures: in-situ structure determination to 1651°C and effect of temperature and bulk composition on the mixing behaviour of structural units. Contrib. to Mineral. Petrol. 117, 1–14. doi:10.1007/BF00307725

Mysen, B.O., Finger, L.W., Virgo, D., Seifert, F.A., 1982. Curve-fitting of Raman spectra of silicate glasses. Am. Mineral. 67, 686–695.

Neuville, D.R., 1992. Etude des Propriétés Thermodynamiques et Rhéologiques des Silicates Fondus. Thèse de l'Université de Paris VII, spécialité Géochimie Fondamentale.

Neuville, D.R., 2005. Structure and properties in (Sr, Na) silicate glasses and melts. Phys. Chem. Glas. 46, 112–118.

Neuville, D.R., 2006. Viscosity, structure and mixing in (Ca, Na) silicate melts. Chem. Geol. 229, 28–41. doi:10.1016/j.chemgeo.2006.01.008

Neuville, D.R., Richet, P., 1991. Viscosity and mixing in molten (Ca, Mg) pyroxenes and garnets. Geochim. Cosmochim. Acta 55, 1011–1019. doi:10.1016/0016-7037(91)90159-3

Neuville, D.R., Mysen, B.O., 1996. Role of aluminium in the silicate network: In situ, high-temperature study of glasses and melts on the join SiO_2-$NaAlO_2$. Geochim. Cosmochim. Acta 60, 1727–1737. doi:10.1016/0016-7037(96)00049-X

Neuville, D.R., Cormier, L., Massiot, D., 2004a. Al environment in tectosilicate and peraluminous glasses: A ^{27}Al MQ-MAS NMR, Raman, and XANES investigation. Geochim. Cosmochim. Acta 68, 5071–5079. doi:10.1016/j.gca.2004.05.048

Neuville, D.R., Cormier, L., Flank, A.M., Briois, V., Massiot, D., 2004b. Al speciation and Ca environment in calcium aluminosilicate glasses and crystals by Al and Ca K-edge X-ray absorption spectroscopy. Chem. Geol. 213, 153–163. doi:10.1016/j.chemgeo.2004.08.039

Neuville, D.R., Cormier, L., Massiot, D., 2006. Al coordination and speciation in calcium aluminosilicate glasses: Effects of composition determined by ^{27}Al MQ-MAS NMR and Raman spectroscopy. Chem. Geol. 229, 173–185. doi:10.1016/j.chemgeo.2006.01.019

Neuville, D.R., Cormier, L., Montouillout, V., Massiot, D., 2007. Local Al site distribution in aluminosilicate glasses by ^{27}Al MQMAS NMR. J. Non. Cryst. Solids 353, 180–184. doi:10.1016/j.jnoncrysol.2006.09.035

Neuville, D.R., Cormier, L., Montouillout, V., Florian, P., Millot, F., Rifflet, J.-C., Massiot, D., 2008a. Structure of Mg- and Mg/Ca aluminosilicate glasses: ^{27}Al NMR and Raman spectroscopy investigations. Am. Mineral. 93, 1721–1731. doi:10.2138/am.2008.2867

Neuville, D.R., Cormier, L., De Ligny, D., Roux, J., Flank, A.M., Lagarde, P., 2008b. Environments around Al, Si, and Ca in aluminate and aluminosilicate melts by X-ray absorption spectroscopy at high temperature. Am. Mineral. 93, 228–234. doi:10.2138/am.2008.2646

Neuville, D.R., Henderson, G.S., Cormier, L., Massiot, D., 2010. The structure of crystals, glasses, and melts along the CaO-Al_2O_3 join: Results from Raman, Al L- and K-edge X-ray absorption, and ^{27}Al NMR spectroscopy. Am. Mineral. 95, 1580–1589. doi:10.2138/am.2010.3465

Neuville, D.R., de Ligny, D., Henderson, G.S., 2014. Advances in Raman Spectroscopy Applied to Earth and Material Sciences. Rev. Mineral. Geochemistry 78, 509–541. doi:10.2138/rmg.2013.78.13

Pasquarello, A., Car, R., 1998. Identification of Raman Defect Lines as Signatures of Ring Structures in Vitreous Silica. Phys. Rev. Lett. 80, 5145–5147. doi:10.1103/PhysRevLett.80.5145

Plazek, D.J., Ngai, K.L., 1991. Correlation of polymer segmental chain dynamics with temperature-dependent time-scale shifts. Macromolecules 24, 1222–1224. doi:10.1021/ma00005a044

Poe, B.T., McMillan, P.F., Cote, B., Massiot, D., Coutures, J.-P., 1994. Structure and Dynamics in Calcium Aluminate Liquids: High-Temperature ^{27}Al NMR and Raman Spectroscopy. J. Am. Ceram. Soc. 77, 1832–1838. doi:10.1111/j.1151-2916.1994.tb07058.x

Rahmani, A., Benoit, M., Benoit, C., 2003. Signature of small rings in the Raman spectra of normal and compressed amorphous silica: A combined classical and ab initio study. Phys. Rev. B 68, 21. doi:10.1103/PhysRevB.68.184202

Ravel, B., Newville, M., 2005. ATHENA, ARTEMIS, HEPHAESTUS: Data analysis for X-ray absorption spectroscopy using IFEFFIT. J. Synchrotron Radiat. 12, 537–541. doi:10.1107/S0909049505012719

Richet, P., 1984. Viscosity and configurational entropy of silicate melts. Geochim. Cosmochim. Acta 48, 471–483. doi:10.1016/0016-7037(84)90275-8

Richet, P., 1987. Heat capacity of silicate glasses. Chem. Geol. 62, 111–124. doi:10.1016/0009-2541(87)90062-3

Richet, P., Bottinga, Y., 1985. Heat capacity of aluminum-free liquid silicates. Geochim. Cosmochim. Acta 49, 471–486. doi:10.1016/0016-7037(85)90039-0

Richet, P., Neuville, D.R., 1992. Thermodynamics of silicate melts: configurational properties, in: Thermodynamic Data. pp. 133–161. doi:10.1007/978-1-4612-2842-4_5

Robie, R.A., Hemingway, B.S., Fisher, J.R., 1978. Thermodynamic Properties of Minerals and Related Substances at 298.15K and 1bar Pressure and at Higher Temperatures, US Geological Survey Bulletin 1452.

Rudnick, R.L., Gao, S., 2003. Composition of the Continental Crust, in: Treatise on Geochemistry. Elsevier, pp. 1–64. doi:10.1016/B0-08-043751-6/03016-4

Scherer, G.W., 1984. Use of the Adam-Gibbs Equation in the Analysis of Structural Relaxation. J. Am. Ceram. Soc. 67, 504–511. doi:10.1111/j.1151-2916.1984.tb19643.x

Seifert, F.A., Mysen, B.O., Virgo, D., 1982. Three-dimensional network structure of quenched melts (glass) in the systems SiO_2-$NaAlO_2$, SiO_2-$CaAl_2O_4$ and SiO_2-$MgAl_2O_4$. Am. Mineral. 67, 696–717.

Sen, P.N., Thorpe, M.F., 1977. Phonons in AX_2 glasses: From molecular to band-like modes. Phys. Rev. B 15, 4030–4038. doi:10.1103/PhysRevB.15.4030

Sharma, S.K., Mammone, J.F., Nicol, M.F., 1981. Raman investigation of ring configurations in vitreous silica. Nature. doi:10.1038/292140a0

Sharma, K., Kothiyal, G.P., Montagne, L., Méar, F.O., Revel, B., 2012. A new formulation of barium–strontium silicate glasses and glass-ceramics for high-temperature sealant. Int. J. Hydrogen Energy 37, 11360–11369. doi:10.1016/j.ijhydene.2012.04.142

Stebbins, J.F., Farnan, I., Xue, X., 1992. The structure and dynamics of alkali silicate liquids: A view from NMR spectroscopy. Chem. Geol. 96, 371–385. doi:10.1016/0009-2541(92)90066-E

Taylor, S.R., 1964. Abundance of chemical elements in the continental crust: a new table. Geochim. Cosmochim. Acta 28, 1273–1285. doi:10.1016/0016-7037(64)90129-2

Thompson, L.M., Stebbins, J.F., 2012. Non-stoichiometric non-bridging oxygens and five-coordinated aluminum in alkaline earth aluminosilicate glasses: Effect of modifier cation size. J. Non. Cryst. Solids 358, 1783–1789. doi:10.1016/j.jnoncrysol.2012.05.022

Turekian, K.K., Kulp, J.L., 1956. The geochemistry of strontium. Geochim. Cosmochim. Acta 10, 245–296. doi:10.1016/0016-7037(56)90015-1

Turekian, K.K., Wedepohl, K.H., 1961. Distribution of the Elements in Some Major Units of the Earth's Crust. Geol. Soc. Am. Bull. 72, 175–192. doi:10.1130/0016-7606(1961)72[175:DOTEIS]2.0.CO;2

Umari, P., Pasquarello, A., 2002. Modeling of the Raman spectrum of vitreous silica: Concentration of small ring structures. Phys. B Condens. Matter 316-317, 572–574. doi:10.1016/S0921-4526(02)00576-8

Urbain G., 1974 Viscosité et structure de silicoalumineux liquides. I. Méthode de mesure et résultats expérimentaux. Rev. Intl. Hautes Temp. Réfract. 11, 133–145.

Urbain, G., Bottinga, Y., Richet, P., 1982. Viscosity of liquid silica, silicates and alumino-silicates. Geochim. Cosmochim. Acta 46, 1061–1072. doi:10.1016/0016-7037(82)90059-X

Ye, Y., Smyth, J.R., Boni, P., 2012. Crystal structure and thermal expansion of aragonite-group carbonates by single-crystal X-ray diffraction. Am. Mineral. 97, 707–712. doi:10.2138/am.2012.3923

Table 1. Chemical composition (in wt%) and density (in g/cm^3) of studied glasses.*

	SA75.12	**SA63.18**	**SA57.21**	**SA50.25**	**SA42.29**	**SA33.33**	**SA26.37**	**SA20.40**	**SA10.45**
SiO_2	62.54(16)	48.59(21)	42.73(9)	36.15(3)	29.72(11)	22.55(15)	16.35(1)	12.96(10)	7.00(4)
Al_2O_3	18.01(9)	24.68(5)	27.36(10)	30.35(4)	33.37(3)	36.88(22)	39.67(8)	41.25(25)	46.08(10)
SrO	19.45(12)	26.73(26)	29.91(19)	33.49(2)	36.91(8)	40.57(37)	43.98(7)	45.78(30)	46.92(29)
Density	2.636(1)	2.837(3)	2.928(12)	3.024(1)	3.132(3)	3.211(2)	3.298(1)	3.359(2)	3.426(2)

* Average of 5-10 analyses made with a Cameca SX100 electron microprobe for each glass at 15 kV and 10 nA with 90 s counting time.

Table 2. Viscosity measurements performed on Sr aluminosilicate glasses. Viscosity is in log(Pa·s) and temperature is in K.

SA75.12		**SA63.18**		**SA50.25**[a]		**SA42.29**		**SA33.33**		**SA26.37**	
T	η	T	η	T	η	T	η	T	η	T	η
1153.1	12.51	1148.9	12.42	1112.0	13.98	1137.0	12.72	1144.8	12.44	1144.2	12.68
1169.5	11.98	1158.9	12.01	1135.0	12.95	1145.3	12.35	1151.1	12.09	1159.2	11.92
1186.3	11.50	1161.3	11.94	1166.0	11.52	1152.6	12.01	1156.4	11.90	1169.2	11.47
1196.4	11.23	1181.4	11.24	1180.0	10.87	1161.3	11.64	1160.6	11.61	1175.2	11.25
1206.7	10.95	1186.6	11.04	1193.0	10.44	1168.5	11.38	1165.7	11.39	1189.2	10.58
1221.4	10.53	1191.3	10.90	1213.0	9.77	1177.3	11.00	1170.8	11.22	1214.2	9.40
1231.3	10.33	1196.2	10.72	1232.0	9.20	1183.3	10.75	1175.9	10.97	1231.2	8.79
1237.7	10.14	1204.8	10.37			1185.6	10.66	1186.9	10.50	1239.2	8.51
1247.1	9.99	1209.2	10.19			1192.9	10.40	1192.0	10.31		
		1219.5	9.92			1201.7	10.09	1206.9	9.81		
		1228.5	9.69			1209.4	9.82	2000.0[b]	-0.20[b]		
		2000.0[b]	0.92[b]			2000.0[b]	0.01[b]	2050.0[b]	-0.36[b]		
		2050.0[b]	0.70[b]			2050.0[b]	-0.17[b]	2100.0[b]	-0.50[b]		
		2100.0[b]	0.51[b]			2100.0[b]	-0.33[b]	2200.0[b]	-0.76[b]		
		2200.0[b]	0.18[b]			2200.0[b]	-0.60[b]				

[a] Measured using a micro-penetration technique.

[b] Interpolated values.

Table 3. T_g and VFTH parameters (A, B, T_1) retrieved from the fitting of low-temperature viscosity data. m is fragility of melts. $C_{p,g}$, $C_{p,l}$, Cp^{conf} and Adam-Gibbs parameters (A_e, B_e, $S^{conf}(T_g)$) determined from the viscosity data presented in Figure 1. See explanation in the text on how the values of $C_{p,g}$ and $C_{p,l}$ were obtained. T_g, T_1, T_0 are in K; $C_{p,g}$, $C_{p,l}$, C_p^{conf}, B_e are in J/mol; A_e is in log(Pa·s), $S^{conf}(T_g)$ is in J/(mol·K).

	SA75.12	**SA63.18**	**SA50.25**	**SA42.29**	**SA33.33**	**SA26.37**	**SA20.40**	**SA10.45**
T_g	1169.2	1159.8	1154.1	1153.0	1153.1	1158.1	1185.8*	1214.0*
A	-5.7944	-14.0710	-6.3440	-8.1320	-9.8495	-20.3770	-	-
B	10614.0	18048.0	7771.7	9314.8	10226.0	21514.0	-	-
T_1	572.7	467.5	730.4	690.3	685.1	493.6	-	-
m	34.9	43.7	49.9	50.2	53.8	56.4	-	-
$C_{p,g}$	77.21	79.58	82.18	83.80	85.56	87.11	88.59	90.91
$C_{p,l}$	88.97	92.46	96.22	98.57	101.14	103.49	106.32	110.64
C_p^{conf}	11.77	12.88	14.04	14.77	15.58	16.38	17.73	19.73
A_e	-2.6425	-2.6278	-3.1003	-3.4952	-3.4188	-3.1614	-	-
10^5 B_e	1.9656	2.2416	3.0132	3.8054	3.9249	3.6818	-	-
$S^{conf}(T_g)$	11.48	13.21	17.29	21.30	22.06	20.96	-	-
T_0	384	647	699	690	742	806	-	-

* T_g value was obtained from DTA measurements

Table 4. Gaussian bands' positions (V_i, cm^{-1}) and areas (A_i, a.u.) obtained from the deconvolution of the high-frequency region of the Raman spectra.

	SA75.12	**SA63.18**	**SA57.21**	**SA50.25**	**SA42.29**	**SA33.33**	**SA26.37**	**SA20.40**	**SA10.45**
V_1	990.1	956.0	936.5	935.2	934.2	923.4	836.9	831.1	813.7
V_2	1099.7	1038.3	1012.5	1003.7	988.9	958.0	939.7	935.4	926.2
V_3	1181.9	1139.8	1117.4	1106.0	1096.0	1046.0	1014.6	1013.1	1007.3
A_1	30.4	23.9	17.2	25.6	22.5	3.2	1.6	4.6	7.6
A_2	50.3	73.5	93.6	102.0	101.9	96.2	72.2	65.5	42.0
A_3	8.8	23.2	31.8	25.0	13.3	25.7	40.8	27.6	15.8

Table 5. ^{27}Al MAS NMR parameters obtained from the deconvolution of the spectra using a Czjzek model. δ_{iso} is isotropic chemical shift (in ppm) and C_Q is quadrupolar coupling constant (in MHz). Population is in %.

	SA75.12	**SA63.18**	**SA57.21**	**SA50.25**	**SA42.29**	**SA33.33**	**SA26.37**	**SA20.40**	**SA10.45**
δ_{iso}									
AlO_4	60.3	62.8	64.1	66.2	68.3	71.3	74.1	76.0	77.8
AlO_5	32.1	34.2	35.0	39.0	40.3	40.0	39.5	41.1	43.4
C_Q									
AlO_4	7.31	7.29	7.00	7.32	7.41	7.45	7.81	8.11	7.53
AlO_5	7.82	7.83	7.13	8.65	8.67	7.62	6.39	6.93	6.81
Population									
AlO_4	97.8	97.1	97.7	95.7	95.5	96.9	98.0	97.8	98.6
AlO_5	2.2	2.9	2.3	4.3	4.5	3.1	2.0	2.2	1.4

Figure captions

Figure 1. Viscosity curves of studied glasses as a function of reciprocal temperature. Lines are VFTH fits. Error bars are less than symbols' size. *Inset*: viscosity data for Sr aluminosilicates plotted versus T_g/T, representing melt's fragility. High-temperature data for SA75.12, SA50.25 and SA26.37 are reproduced from Urbain et al. (1982) and viscosities for the intermediate compositions were estimated linearly from the end-members. Lines are only guide for the eye.

Figure 2. T_g versus silica content. Points for SA10.45 and SA20.40 compositions were obtained using DTA. Error bars are less than the size of symbols except for SA10.45 and SA20.40 for which they were reasonably set at ±5 K level. Line is a guide for the eye. A dashed part of the line shows expected behaviour of T_g curve in the region of 75-100 mol% of SiO_2 (no experimental data available for the SAS system). T_g of 1473 K for vitreous silica is from Bruckner (1970).

Figure 3a. Uncorrected normalized Raman spectra of Sr tectosilicate glasses. SiO_2 spectrum corresponds to one of INF302 silica glass.

Figure 3b. Boson peaks of uncorrected spectra of SAS glasses. The line shows a trend in the evolution of a Boson peak with changing composition.

Figure 4a. Deconvolution of the high-frequency region of corrected and normalized Raman spectra of SAS glasses. Orange bands are related to T_{2s} vibrational mode, blue and green ones – to vibrations of $Q^{4,II}$ and $Q^{4,I}$ species, respectively.

Figure 4b. Dependence of Raman shift of Gaussian bands on silica content obtained from fitting of the high-frequency region of Raman spectra. ◪ – T_{2s} vibrational mode, ■ – vibrations of $Q^{4,II}$ species, ◩ – vibrations of $Q^{4,I}$ species. Information on vitreous SiO_2 (black symbols) is from Mysen et al (1982). Orange symbols correspond to Na tectosilicates (Neuville and Mysen, 1996), blue symbols correspond to Mg tectosilicates (Neuville et al., 2008a) and green symbols correspond to Ca tectosilicates (Neuville et al., 2004a). New data on Sr aluminosilicates are represented by red symbols. Lines are only guide for the eye.

Figure 5. *Left*: 1D ^{27}Al Quantitative 1 pulse MAS NMR of studied glasses. A shift to higher values of δ_{iso} is clearly visible. *Right*: Deconvolution of the ^{27}Al NMR spectrum for SA50.25 using the GIM model (Massiot et al., 2002). Black solid line is the original spectrum, red dashed line is the sum, blue solid line – the signal from AlO_4 sites, blue dashed line with asterisk – a spinning side band, green solid line – the signal from AlO_5 sites.

Figure 6a. Evolution of isotropic chemical shift δ_{iso} of $Al^{[4]}$ and $Al^{[5]}$ for SAS (red), CAS (green, Neuville et al., 2004a) and MAS (blue, Neuville et al., 2008a) glasses. Error bars are less than symbols' size.

Figure 6b. Population of $Al^{[5]}$ in SAS (red), CAS (green, Neuville et al., 2004a) and MAS (blue, Neuville et al., 2008a) glasses. Lines are only guide for the eye.

Figure 7. XANES spectra at the Sr K-edge for Sr tectosilicate glasses with a crystalline standard ($SrCO_3$).

Figure 8. $S^{conf}(T_g)$ as a function of SiO_2 content. Line is a guide for the eye. Error bars was set as ±5 % after Neuville and Richet (1991).

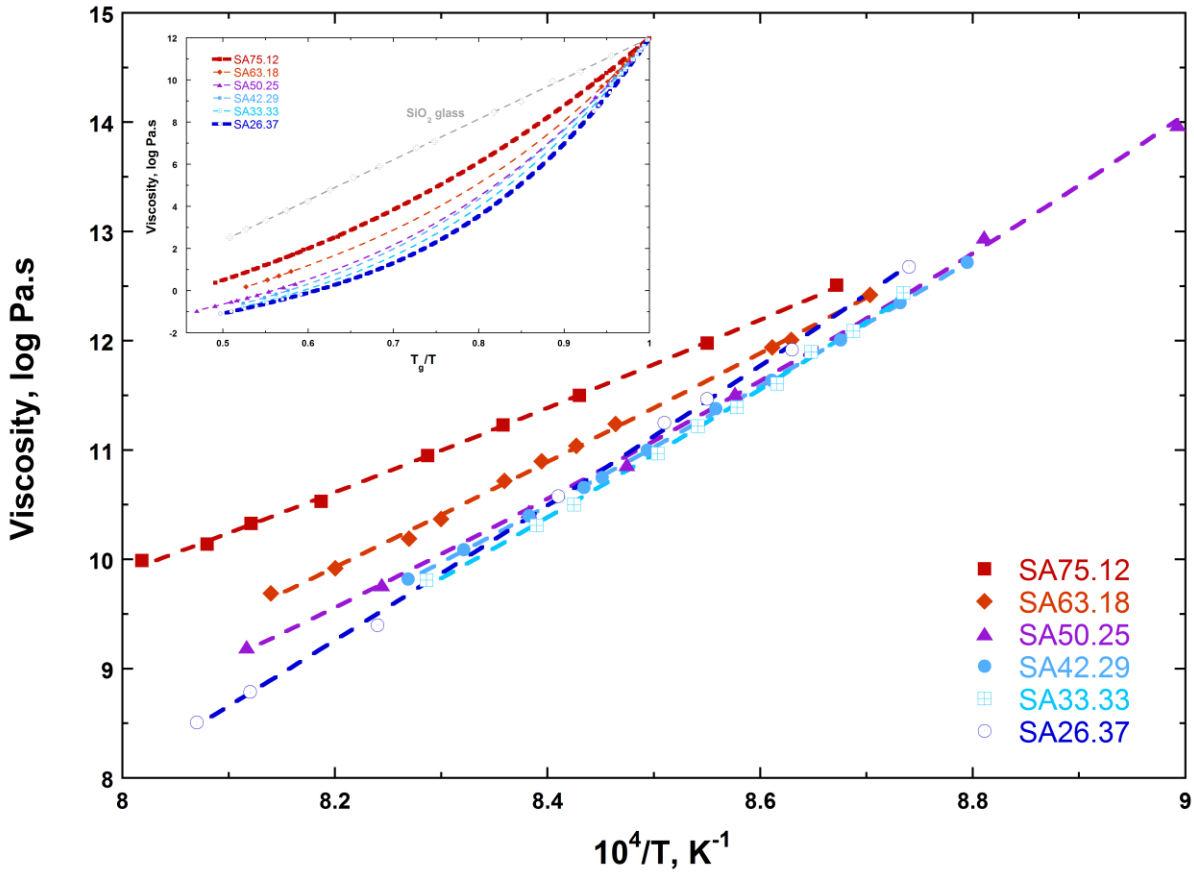

Fig. 1

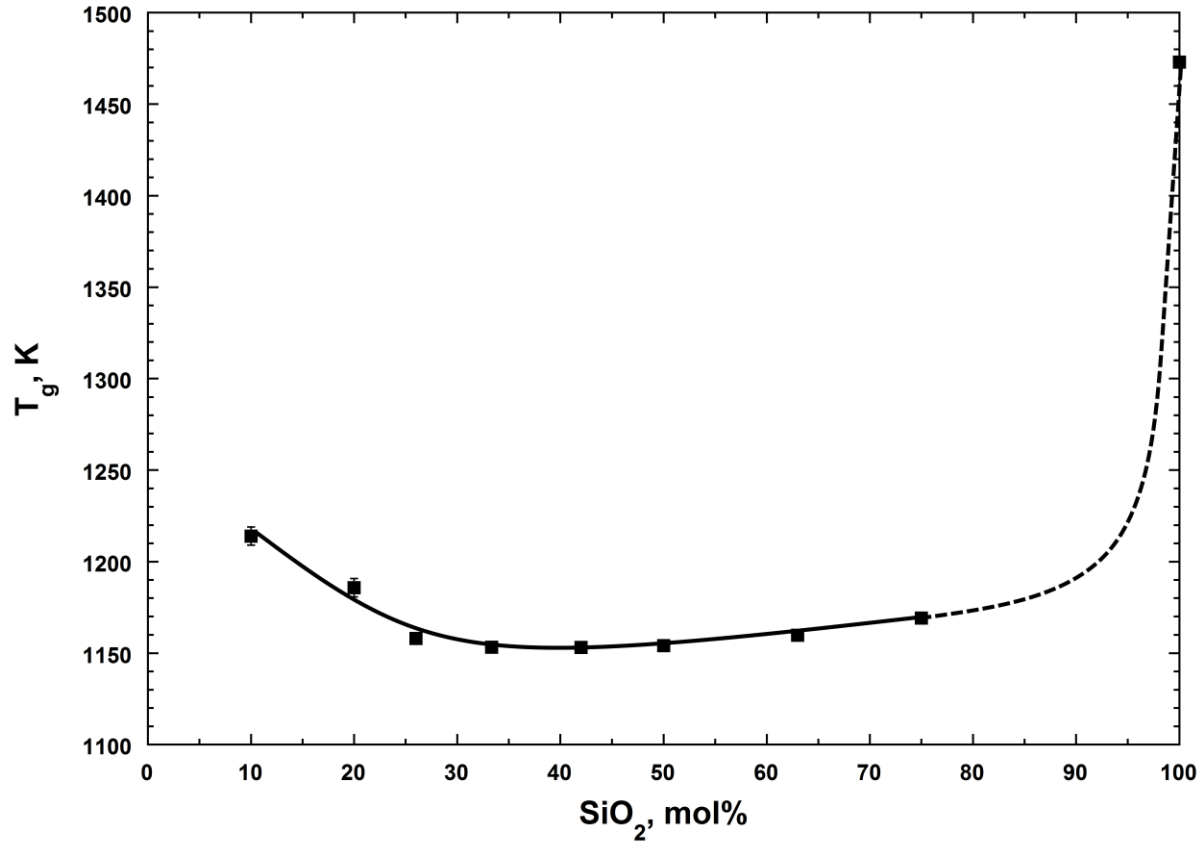

Fig. 2

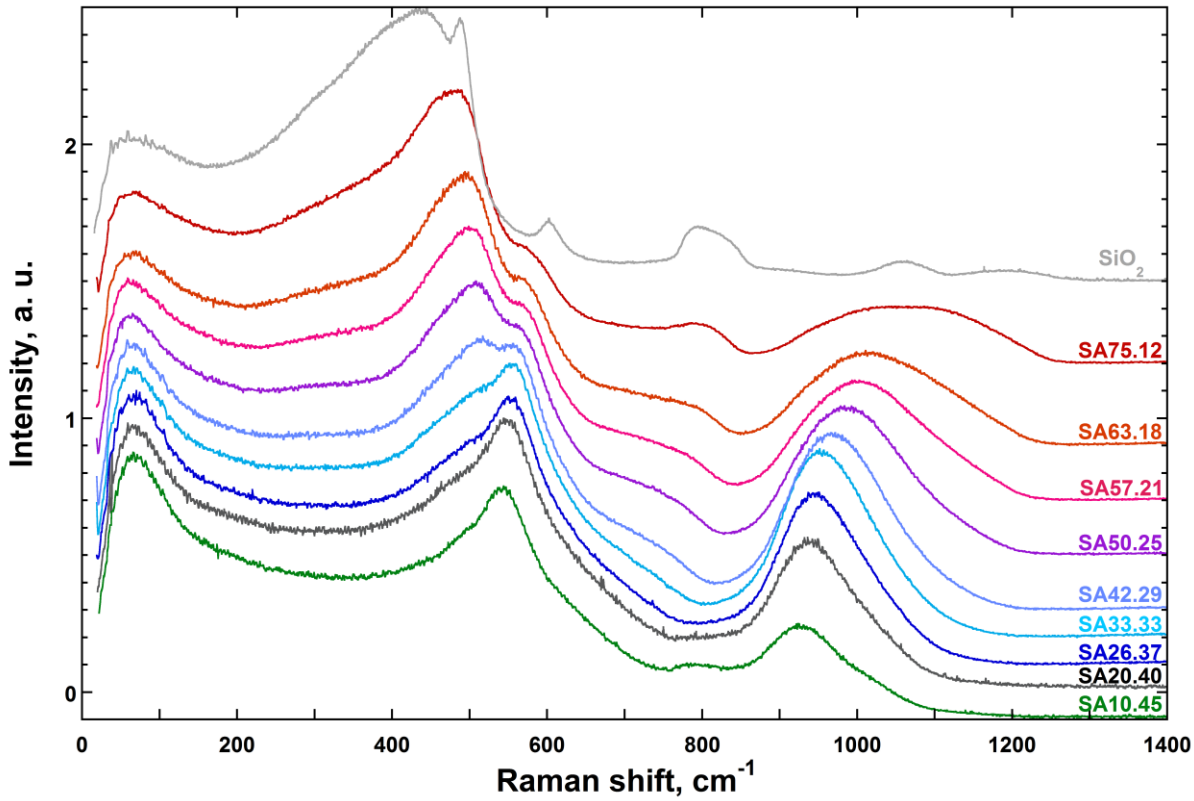

Fig. 3a

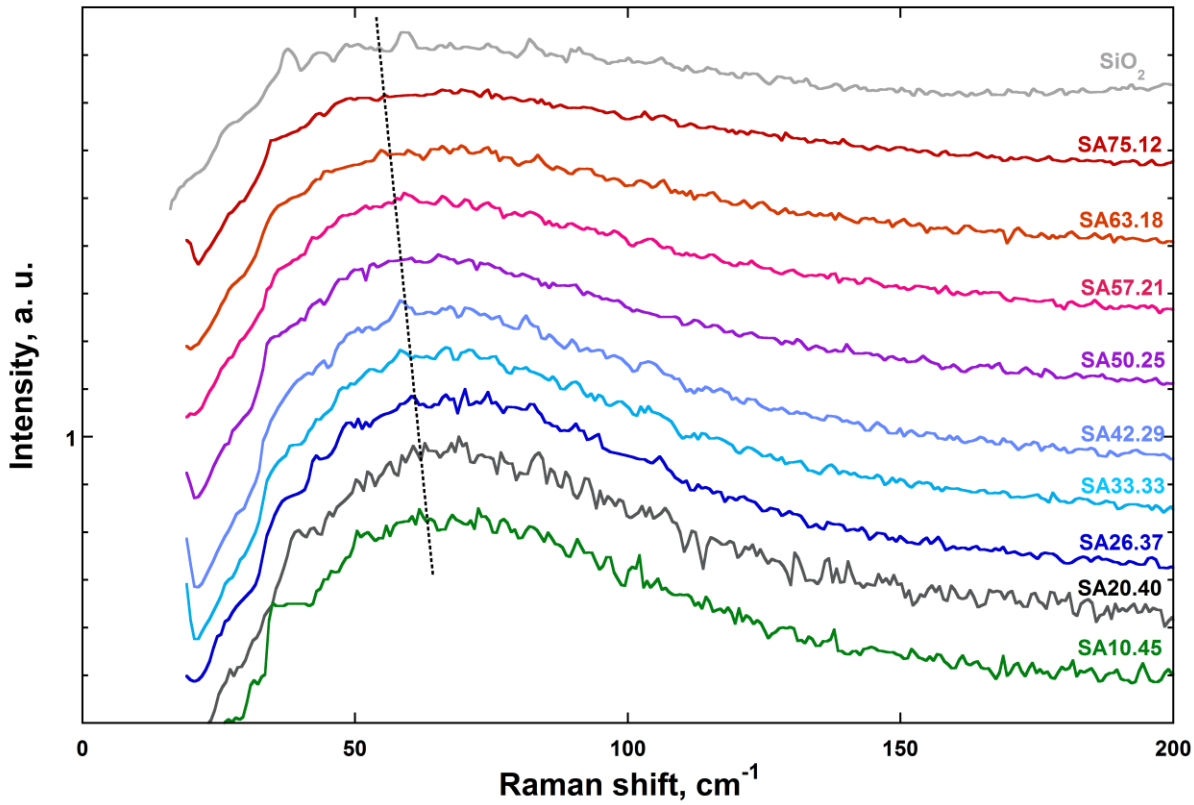

Fig. 3b

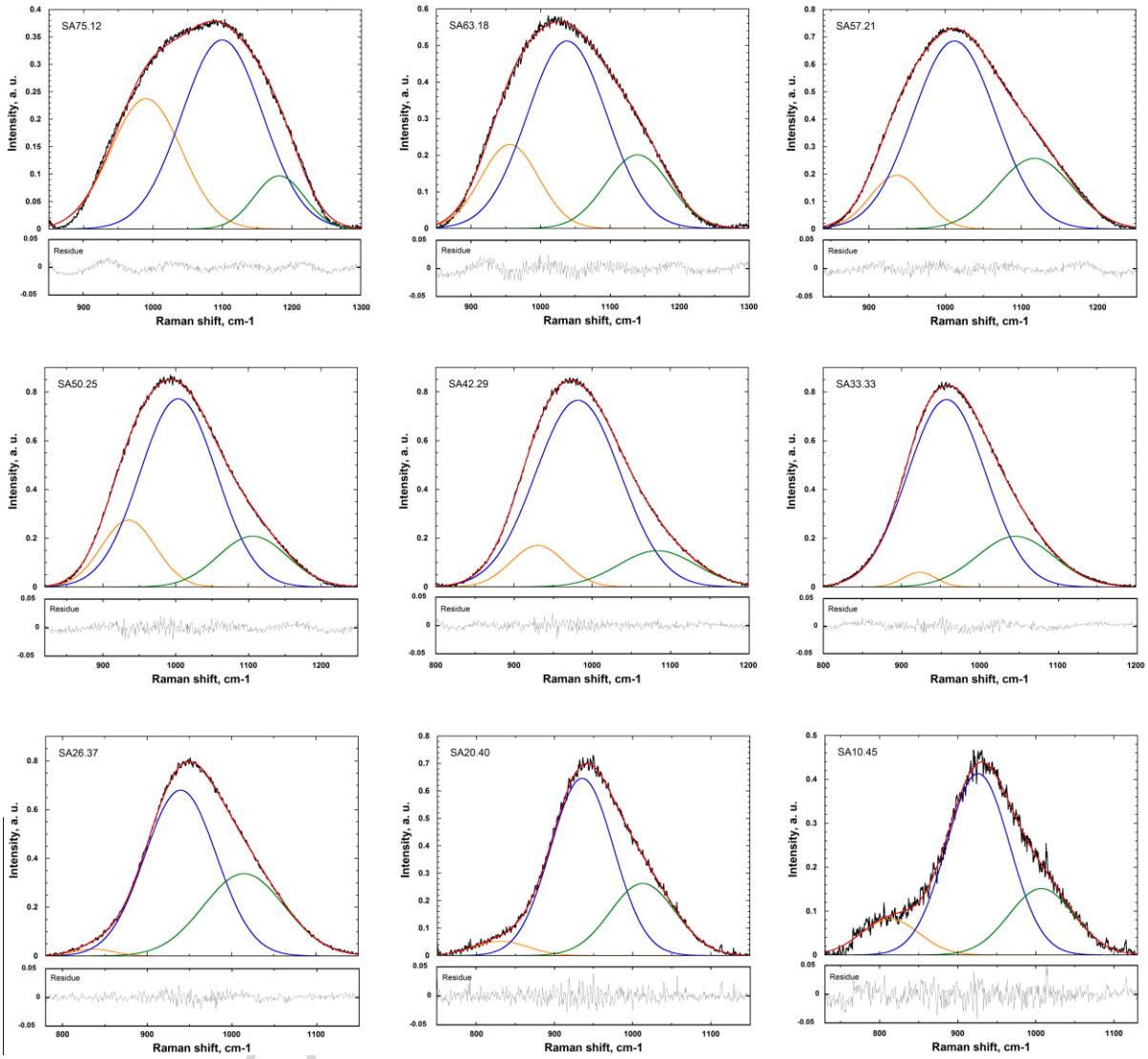

Fig. 4a

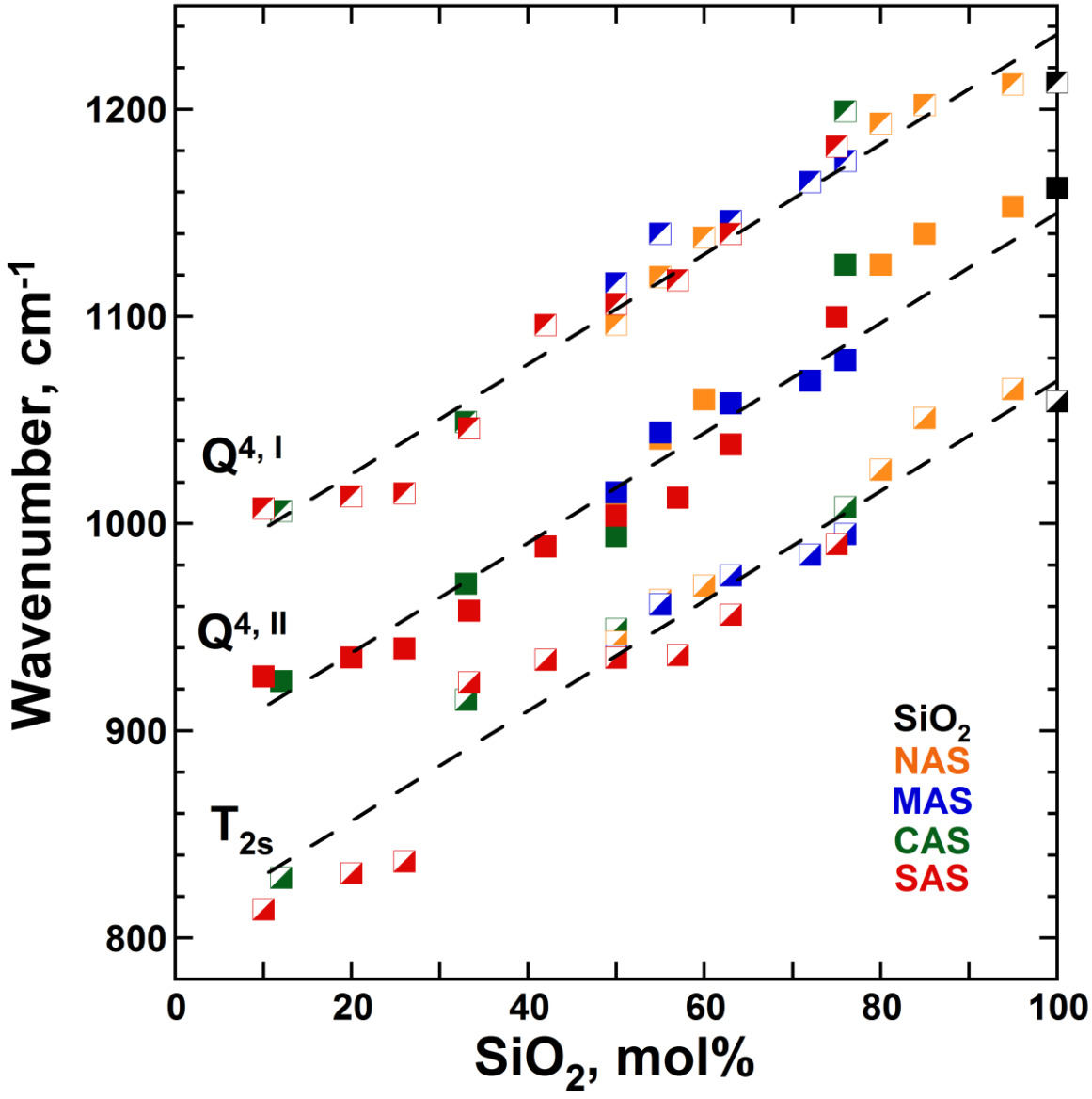

Fig. 4b

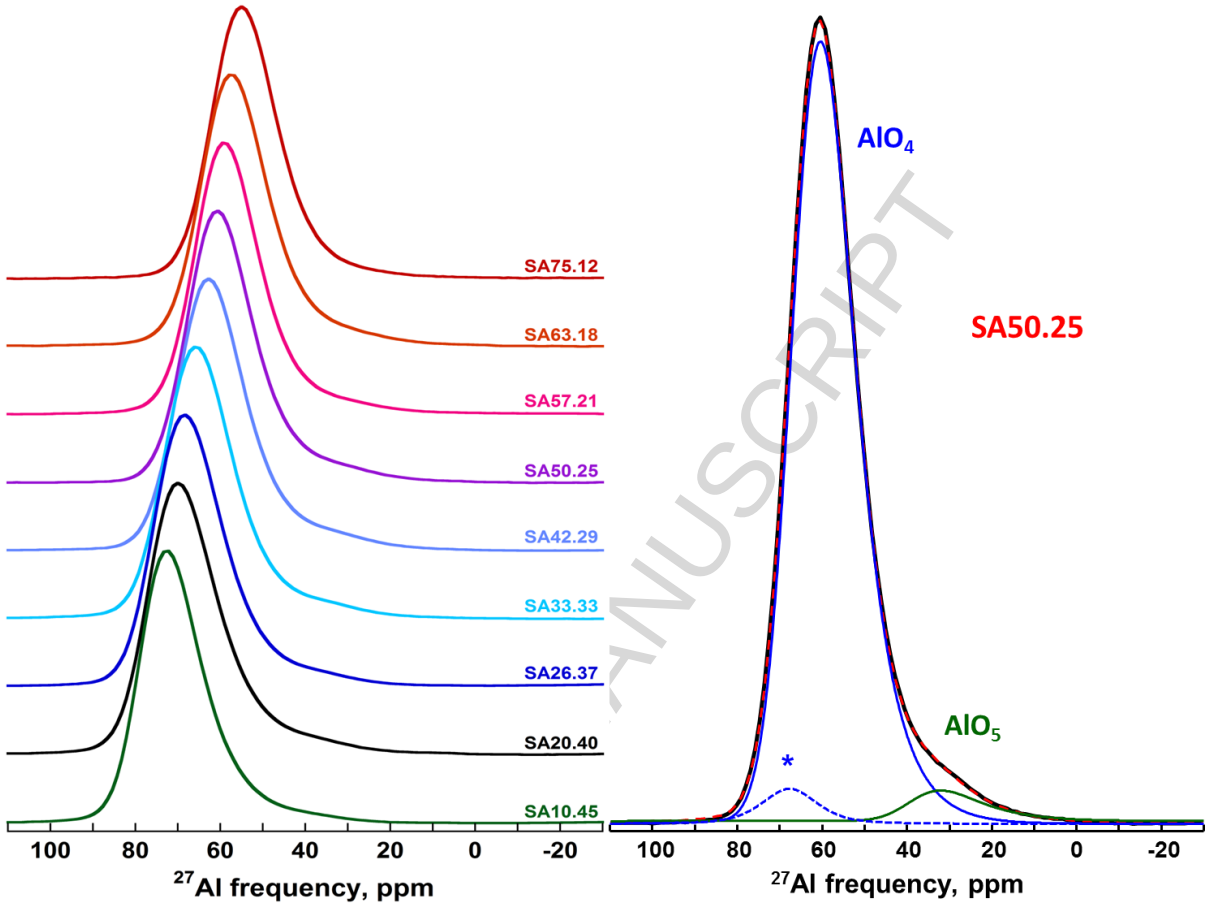

Fig. 5

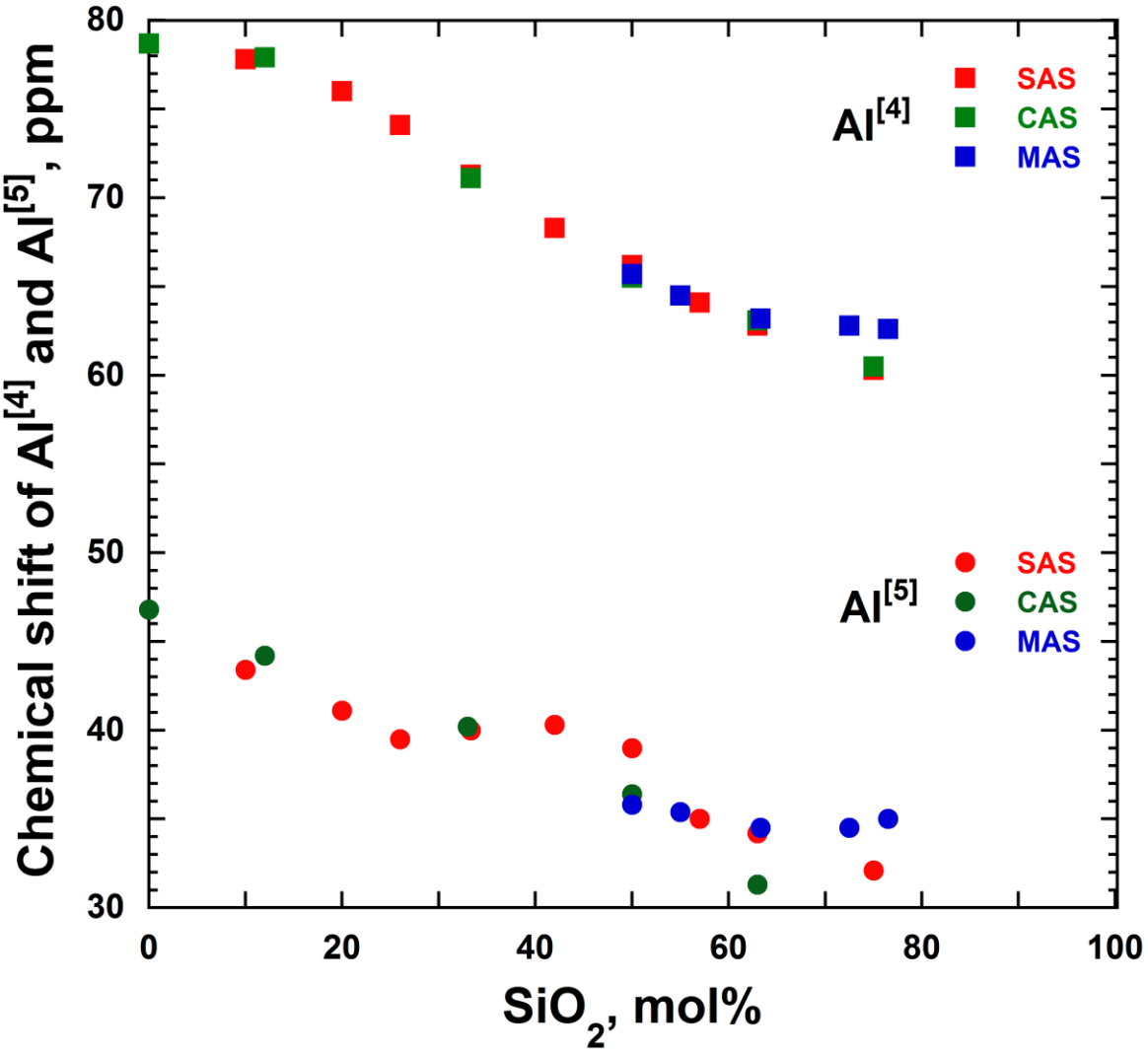

Fig. 6

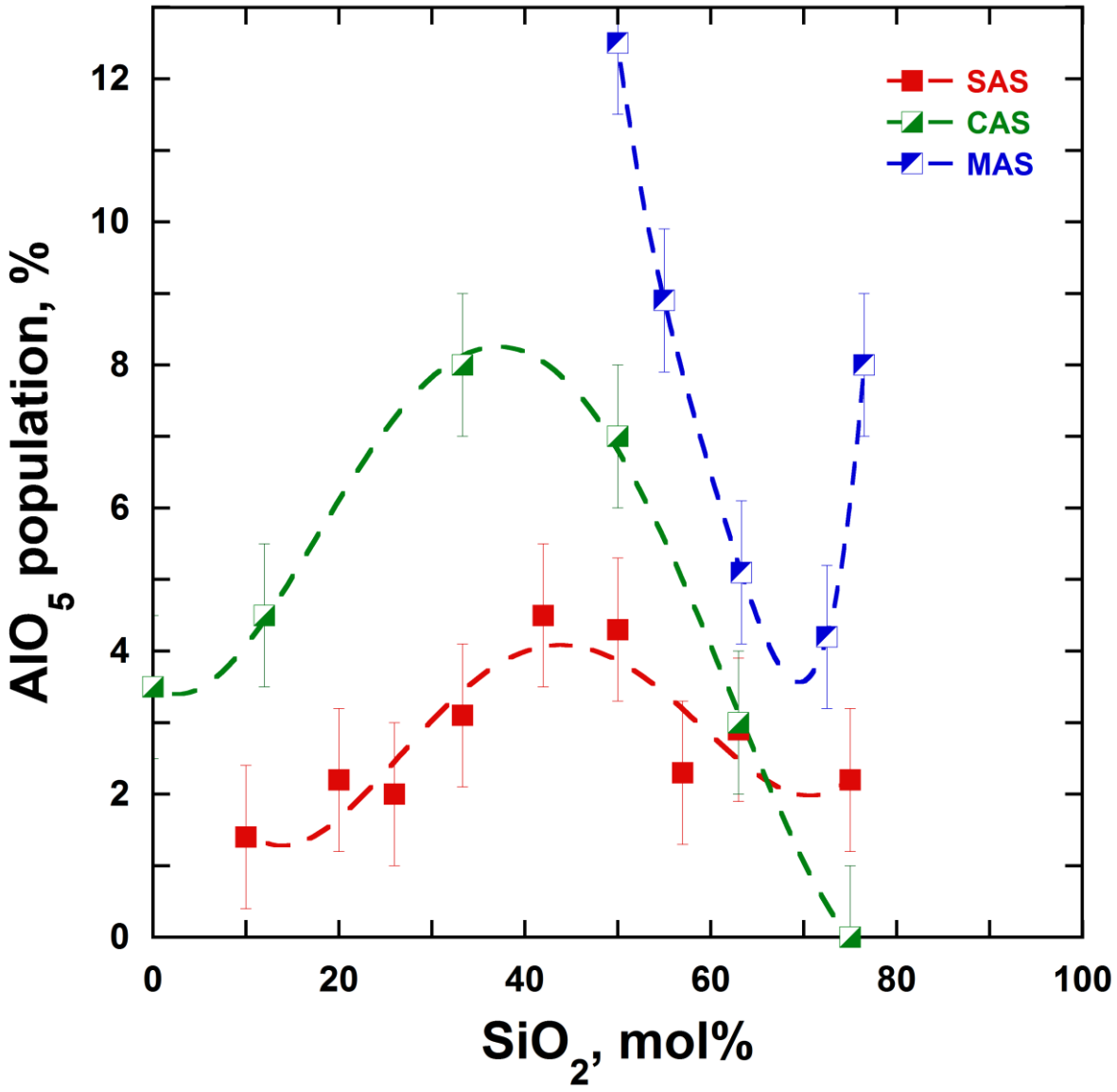

Fig. 6a

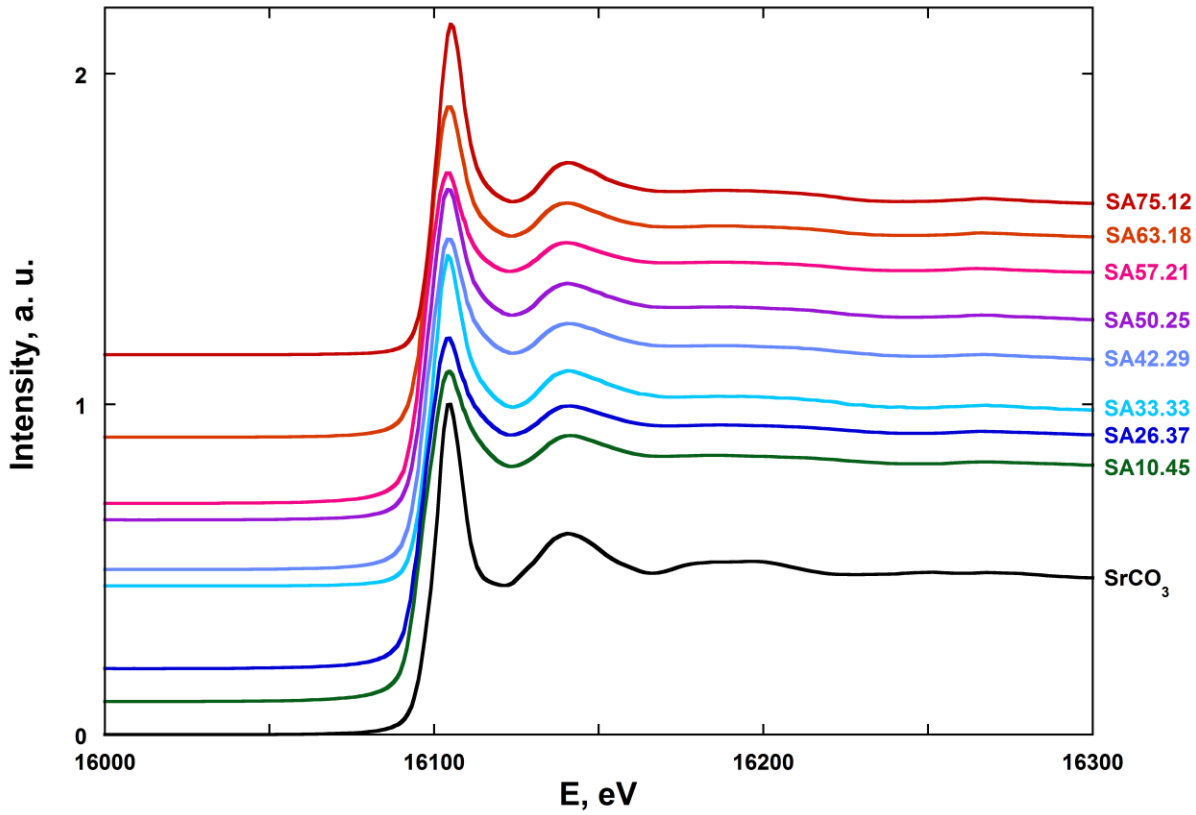

Fig. 7

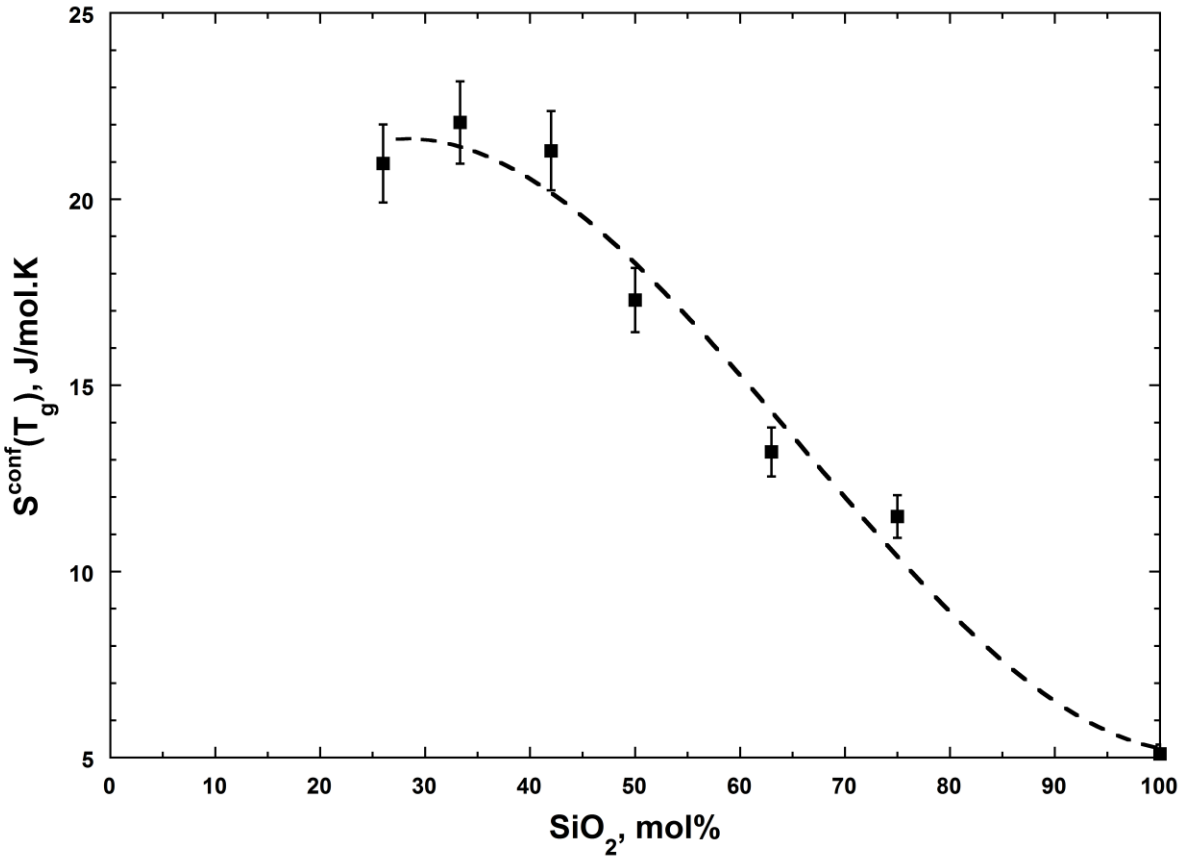

Fig. 8